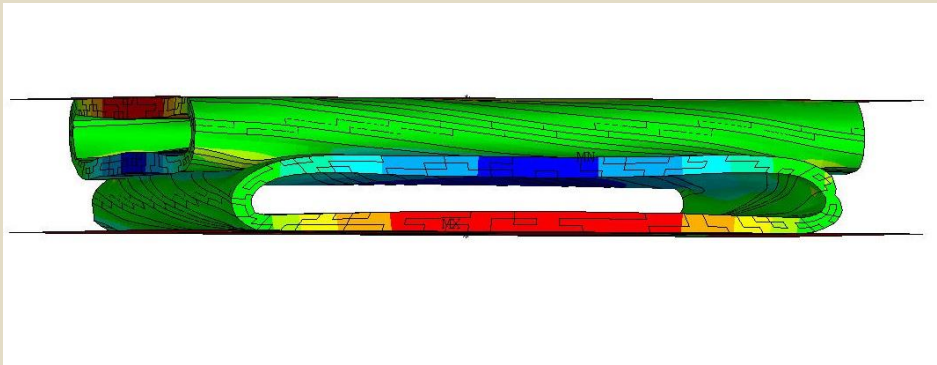


Micromechanical Numeric Investigation of Fiber Bonds in 3D Network Structures

YAĞIZ AZİZOĞLU



KTH Engineering Sciences

Master of Science Thesis
In Solid Mechanics
Stockholm, Sweden 2014



KTH Engineering Sciences

Micromechanical Numeric Investigation of Fiber Bonds in 3D Network Structures

Yağız Azizoğlu

Supervisor: Assoc. Prof. Artem Kulachenko

Master of Science Thesis, 2014
KTH School of Engineering Sciences
Department of Solid Mechanics
Royal Institute of Technology
SE-100 44 Stockholm Sweden

Abstract

In manufacturing of paper and paperboard, optimized fiber usage has crucial importance for process efficiency and profitability. Dry strength of paper is one of the important quality criteria, which can be improved by adding dry strength additive that affect fiber to fiber bonding. This study is using the micromechanical simulations which assist interpretation of the experimental results concerning the effect of strength additives.

A finite element model for 3D dry fiber network was constructed to study the effect of bond strength, bond area and the number of bonds numerically on the strength of paper products. In the network, fibers' geometrical properties such as wall thickness, diameter, length and curl were assigned according to fiber characterization of the pulp and SEM analyses of dry paper cross-section. The numerical network was created by depositing the fibers onto a flat surface which should mimic the handsheet-making procedure. In the FE model, each fiber was represented with a number of quadratic Timoshenko beam elements where fiber to fiber bonds were modelled by beam-to-beam contact. The contact model is represented by cohesive zone model, which needs bond strength and bond stiffness in normal and shear directions. To get a reasonable estimate of the bond stiffness, a detailed finite element model of a fiber bond was used. Additionally, the effect of different fiber and bond geometries on bond stiffness were examined by this model since the previous work [13] indicated that the bond stiffness can have a considerable effect on dry strength of paper.

The network simulation results show that the effect of the strength additive comes through improving the bond strength primarily. Furthermore, with the considered sheet structure, both the fiber bond compliance and the number of bonds affect the stiffness of paper. Finally, the results of the analyses indicated that the AFM measurements of the fiber adhesion could not be used directly to relate the corresponding changes in the bond strength.

The fiber bond simulation concluded that fiber wall thickness has the most significant effect on the fiber bond compliance. It was also affected by micro-fibril orientation angle, bond orientation and the degree of pressing.

Keywords: Finite element, strength additive, 3D model, fiber network model, contact stiffness, paper strength, AFM, fiber adhesion.



KTH Teknikvetenskap

Mikromekanisk Numerisk Studie av Fiberbindning i 3D Fibernätverksmodell

Yağız Azizoğlu

Handledare: Assoc. Prof. Artem Kulachenko

Examensarbete i Hållfasthetslära
Avancerad nivå, 30 hp
Stockholm, Sverige 2014

Sammanfattning

I tillverkningen av pappersprodukter är optimeringen av fiberanvändningen av stor vikt både i tillverkningsprocessen och för ökad vinst. En av de viktigaste kvalitetskriterierna är papperets styrka i torrt tillstånd, vilket kan förbättras genom att tillsätta torrstyrkemedel som påverkar fibrerna och deras bindningar till varandra vid papperstillverkningen. I denna studie används en mikromekanisk modell för att kunna jämföra experimentella resultat rörande effekten av styrkemedel.

En 3D finit element (FE) modell av fibernätverket i torrt tillstånd konstruerades för att numeriskt studera effekten av bindningsstyrkan, bindningsarean och antalet bindningar på papperets styrka. I fibernätverksmodellen så tilldelades fibrerna geometriska egenskaper, så som väggjocklek, diameter, längd och form utifrån fiberkaraktärisering och SEM analys av papperets tvärsnitt i torrt tillstånd. Det numeriska fibernätverket skapades genom att med en depositionsteknik placera fibrer på en plan yta vilket ämnar härma tillverkningen av pappersark. I finita element (FE) modellen så representeras varje fiber av ett antal kvadratiske Timoshenko balkelement där bindningen mellan två fibrer modellerades med kontakt mellan balk elementen. Kontaktmodellen är representerad av en kohesiv-zon modell, vilken kräver bindningsstyrka och bindningsstyvhet i både normal- och skjuvriktningen. För att få en rimlig uppskattning av bindningsstyvheten så används en detaljerad finit element (FE) modell av en bindning mellan två fibrer. Vidare så studerades effekten av olika fiber- och bindningsgeometrier på bindningsstyvheten eftersom föregående studier [13] visar på att bindningsstyvheten kan ha stor inverkan på papperets styrka i torrt tillstånd.

Resultaten från simuleringarna av fibernätverket visar att styrkemedel främst har en effekt på bindningsstyrkan. I den aktuella pappersarkstrukturen så påverkar både fiberbindningskompliansen och antalet bindningar papperets styvhet. Slutligen, resultaten visar att AFM mätningarna av fiberbindningsstyrkan (adhesion) inte kan användas direkt för att relatera de motsvarande ändringarna i bindningsstyrkan.

Slutsatsen av simuleringarna av fiberbindningarna är att fibrernas väggjocklek har den största inverkan på fiberbindningskompliansen vilken också var påverkad av mikrofibrillorienteringen, bindningsorienteringen och mängden pressning av nätverket.

Acknowledgments

The work presented in this thesis was carried out in BiMaC Innovation center at the Department of Solid Mechanics, Royal Institute of Technology (KTH), Stockholm. The project was carried out for the leading paper-making company Stora Enso, that provided the financial support, which is gratefully acknowledged.

I would like to thank my supervisor Associate Professor Artem Kulachenko for his excellent guidance and support as well as for personal advices to become a good engineer during the course of this work. Without his support and encouragement, this work would most probably not have been completed. I would also like to thank my deputy supervisors, Mats Fredlund and Göran Niklasson from Stora Enso for involving me into the project, and all the support to improve the work.

I am thankful to Kurosh Motamedian for spending so much time with me, giving me valuable suggestions and being participant to improve the fiber network generation. Thanks are also due to Svetlana Borodulina, Innventia and the department of Fibre and Polymer Technology (KTH) for the support in the experimental works.

I wish to extend my thanks to my friends, Sofia Sandin for the linguistic advice regarding the manuscript and both Sofia and Marta Björnsdóttir for making my life in Sweden easier.

Stockholm, February 2014.

Yağız Azizoğlu

Contents

INTRODUCTION.....	13
1.1 General remarks	13
1.2 Project objective	13
1.3 Previous work	14
1.4 Thesis overview	14
EXPERIMENTS.....	17
2.1 Fiber characterization.....	17
2.2 SEM image analyses	18
2.3 AFM test	21
2.4 Tensile Test.....	22
2.4.1 Materials	23
2.4.2 Methods	23
2.4.3 Results	23
2.4.4 Observations	25
2.5 Digital Speckle Photography (DSP)	26
FE FIBER BOND SIMULATION	29
3.1 Problem definition	29
3.2 Geometry	30
3.3 Material	32
3.4 Mesh.....	33

3.5	Boundary conditions	35
3.6	Computational experiment	35
3.7	Results.....	36
	Part 1: Parametric study.....	36
	Part 2: Model for network simulation.....	42
	3D DRY FIBER NETWORK SIMULATION	47
4.1	Network generation	47
4.1.1	Fiber cross-section	47
4.1.2	Fiber curl.....	48
4.1.3	Fiber disposition	48
4.1.4	Fiber on 3D space	49
4.1.5	Network thickness.....	50
4.2	FE network model	52
4.2.1	Fiber model	53
4.2.2	Contact model	53
4.2.3	Material	54
4.2.4	Boundary conditions	54
4.2.5	Results	55
	DISCUSSION AND CONCLUSIONS	61
5.1	Future work	62
	REFERENCES.....	63
	APPENDIX.....	65

Part 1

Introduction

1.1 General remarks

Paper is the one of the most consumed industrial product in various fields. Paper is essentially a network of pressed fibers which are held together by hydrogen bonds. The hydrogen bonding is the main mechanism allowing fibers to adhere to each other in the dry state. Apart from the fiber alignment, the mechanical properties of the paper are mainly controlled by the bond and the fiber properties. The fibers are obtained by pulping wood. The pulping process can be done by chemical, mechanical and combined chemical-mechanical methods depending on the produced grade.

Dry strength is one of the important paper quality criteria. It can be affected by strength additives which improve the fiber-fiber bond strength. Another way to increase paper strength is pulp beating, which softens the fiber wall and improves bonding as well. While comparing the effect of these two methods, one should carefully evaluate the impact of other factors such as density, sheet formation, fines retention and wet pressing. Thus, direct comparison of the effect of additives versus mechanical beating experimentally is problematic without a critical evaluation of the mechanism underlying the strength changes.

This study is using the micro-mechanical simulations which assist interpretation of the experimental results concerning the effect of strength additives.

1.2 Project objective

The main focus on the project is examining the influence of dry strength additive on fiber bonds in a paper structure by developing a 3D fiber network simulation. This mechanical model will give us a possibility to investigate the effect of bond strength, bond area and the number of bonds on the strength in the same fiber network structures which have completely the same fiber geometries, materials, and orientations in the networks. Investigating the influence on these parameters in the same network will assist experimental method in terms of excluding the effect of stochastic nature of paper and mutual interference of the paper-making parameters.

In the project, we realized the following points.

- 1) Creating realistic network structure by numerical deposition technique in Fortran.
- 2) Constructing the detailed bond model of two fibers to obtain the bond stiffness in normal and shear direction by finite element (FE) simulation.
- 3) Studying the effect of different fiber and bond geometries on bond stiffness by FE simulation.
- 4) Performing 3D FE network simulation by using the realistic network structure from Fortran and bond stiffness of the FE bond model.
- 5) Parametric study on how the network strength is affected by the bond strength, bond area, the number of bonds and their variability.

1.3 Previous work

In 1983, Seth and Page presented probably one the most cited study of how relative bonded area (RBA) and the bond strength affect the paper strength [1]. In 1997, Gurnagul and Seth showed that mechanical properties of the fiber are heavily controlled by fiber-fiber interaction and single fiber properties [2]. Retulainen and Nieminen (1996) [3], worked on the effect of dry strength additive on tensile strength of paper for several strengthening. Later, Niskanen et al [4] and [5] presented a series of studies based on numerical representation of the network and studied the elastic properties and strength of 2D networks [6] and [7] putting the existing theoretical models to the test.

Although 2D models are computationally effective, they are unable to capture real connectivity in the network, which is undoubtedly important. In 2000, Heyden [8] and in 2002, Gustafsson [9] modeled 3D fiber network model by depositing the fibers randomly in a volume.

Kulachenko and Uesaka, [11] extended Heyden's model by introducing the fiber-to-fiber contact model through a point-wise beam-to-beam contact elements [12]. Borodulina and Kulachenko [13] studied the dry strength of thin sheet using the model and, concluded among other things, the tangent compliance of the bond region is an important factor affecting the network strength. We will use the model originally developed by Kulachenko and Uesaka and investigate the factors and the fiber properties which affect the bond compliance.

1.4 Thesis overview

In Part 2, following the introduction, we present the experimental results from fiber characterization, SEM image analyses, tensile test and AFM measurement. We used fiber characterization results from FiberLab and SEM image analyses to reconstruct the network numerically. By using SEM image analyses we estimated the shrinkage factor as the thickness data received by FiberLab was sampled from wet fibers. In addition, we used SEM images of paper cross-section to compare with cross-section of the network

simulation in terms of number of fibers. AFM result was used to investigate the effect of additive on bond strength. Finally, we used the tensile test result to assess the effect of strength additives and compare the results with finite element model.

In Part 3, we present an extensive study with a detailed finite element model of a fiber bond. We calculated the bond stiffness with geometries matching those from fiber characterization. The stiffness in normal and shear directions were later used in the fiber network model. Since the bond stiffness is one of the important parameters, which affects the paper strength, we conducted a parametric study investigating the effect of fiber diameter, wall thickness, micro fibril orientation angle, contact angle, initial shape, relatively bonded area (RBA), inner bonded case, and effect of maximum press force on bond stiffness.

In Part 4, we present an algorithm used for generating the network. We present the fiber density profile of the generated network in the thickness direction, and develop an algorithm that calculates network thickness. We compared the cross-section of the generated network with SEM image. We presented the tensile test results from the simulation and performed parametric studies.

In Part 5, we present conclusion and suggestions for future work.

Appendices contain a user manual of speckle photography setup.

Part 2

Experiments

2.1 Fiber characterization

We sent CTMP pulp samples used in considered paper samples to Papiertechnische Stiftung (PTS) for the characterization. We used the result of the fiber characterization to design the 3D fiber network simulation to be able to obtain the network with fiber characterizing matching the test sample.

In the table below we presented the mean values of the fiber characterization result.

Table 2.1: Mean values of the fiber dimensions.

Diameter (μm)	Wall thickness (μm)	True length (mm)	Projected length (mm)	Shape factor (-)
29.9	9.2	0.7	0.7	1

Figures, 2.1 and 2.2 show the distribution of the fiber geometries.

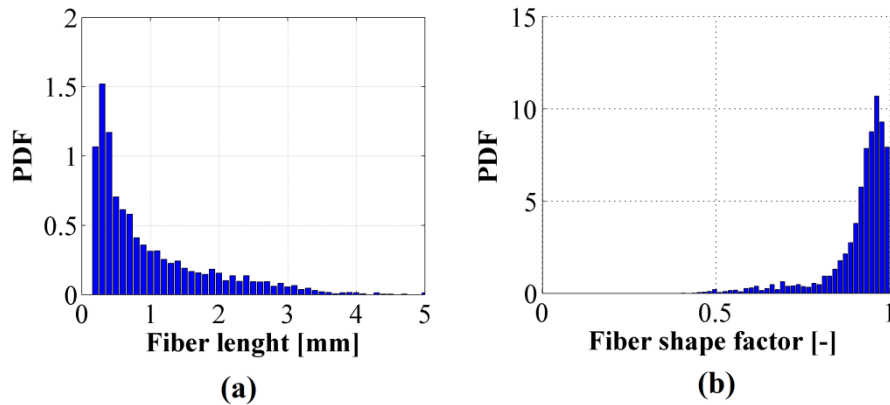


Figure 2.1: a) Fiber length distribution b) Fiber shape factor distribution.

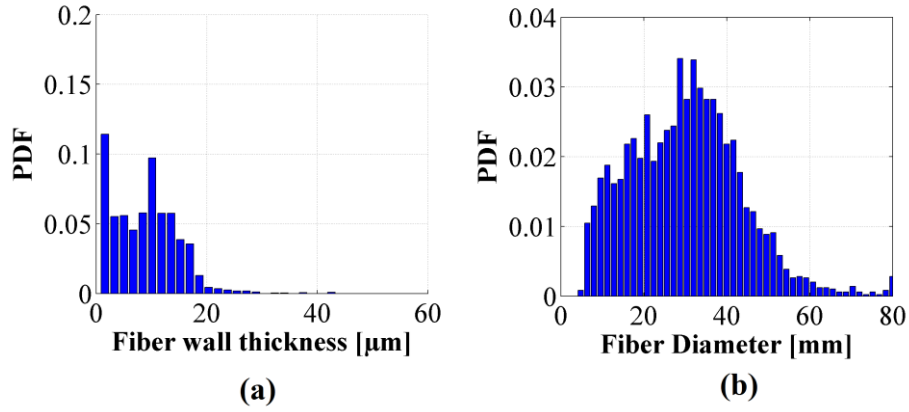


Figure 2.2: a) Fiber wall thickness distribution b) Fiber diameter distribution.

The mean value of the fiber wall thickness is fairly high compared to CTMP wall thickness reported in the literature, which is normally between 2-4.5 μm [14]. The obvious reason of that is the test was performed when the fibers were wet. Therefore, the measured diameter as well as the wall thickness cannot be used for generating the fibers network for studying the dry strength. Therefore, we decided to extract the fiber diameter and the wall thickness from the SEM images of the handsheets.

2.2 SEM image analyses

We took several SEM images of the cross section from the paper sample with the help of Innventia AB, who prepared the cross-sections and KTH- Fiber and Polymer Technology lab, who granted the access to SEM equipment. Figure 2.3 shows an example of the extracted image.

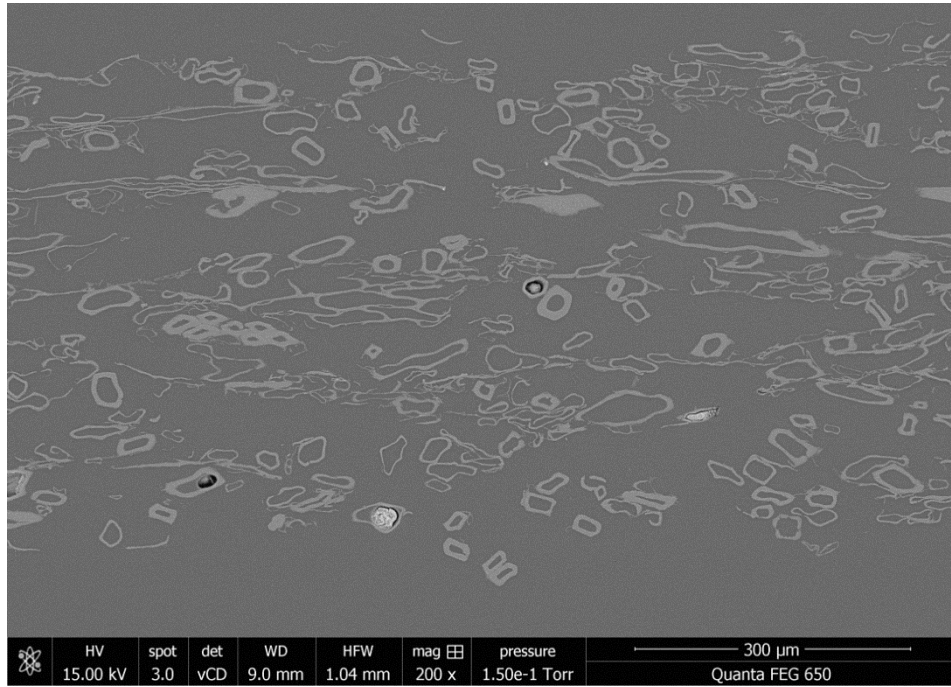


Figure 2.3: SEM image of paper cross section.

After filtering and post-processing, we used the cross section images to find the wall thickness and diameter distribution of the fibers. *ImageJ* image analyses software was used in the analyses. The filtered image used in the analysis is shown in Figure 2.4 where we denoted the fibers cross-section used in the measurements.

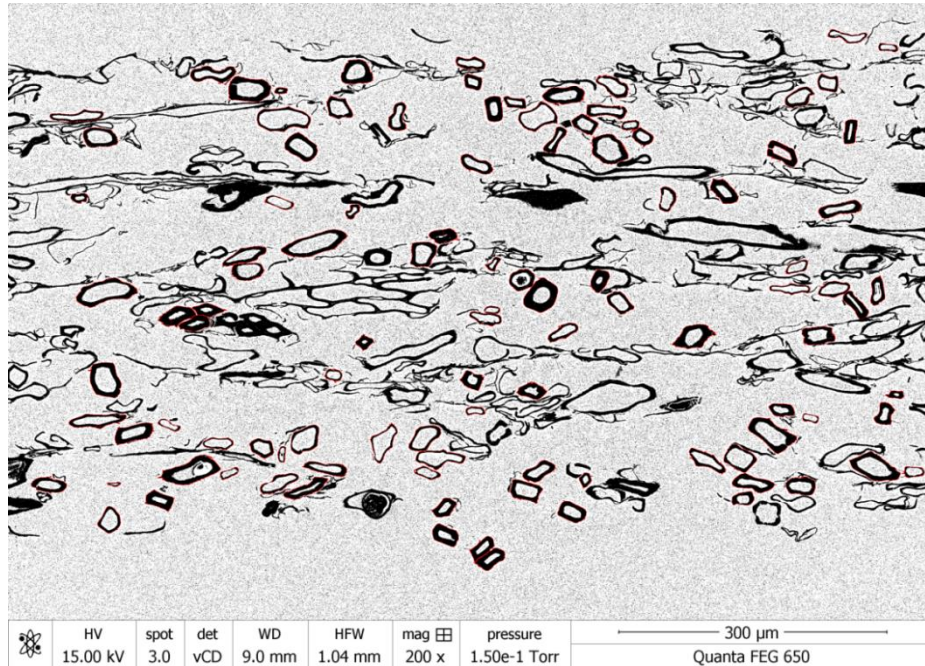


Figure 2.4: Analyzed SEM image with *ImageJ*.

In the analyses, we measured inner diameter, outer diameter and wall thickness of totally 234 fiber cross-sections. The wall thickness distribution as percent of diameter and the diameter distributions from the image analyses are shown in the Figure 2.5.

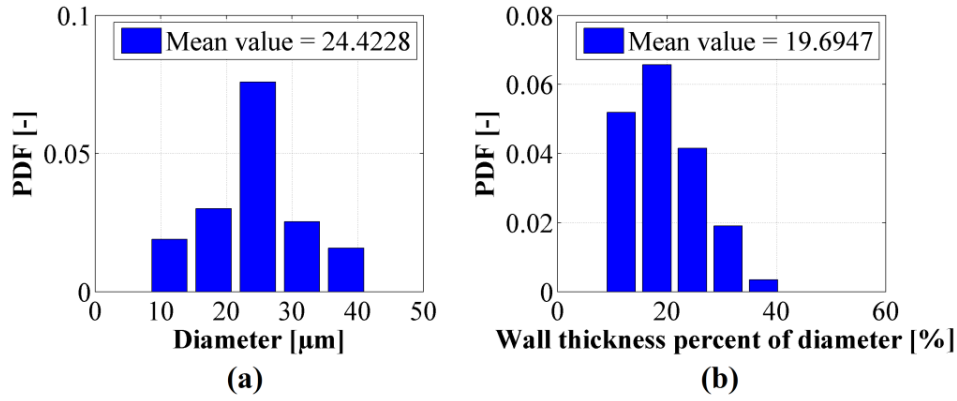


Figure 2.5: a) Fiber diameter distribution b) Fiber wall percentage distribution.

According to this distribution, the mean value of wall thickness is 4.8 μm which is half of the wet fiber measured by FiberLab. We re-scale all the wet fiber diameters from fiber characterization. By using re-scaled diameter values, we generated a fiber network and the total thickness of the network decreased by 20% as compared to the wet state. This is fairly consistent with average transversal shrinkage of a paper [15], (see Figure 2.6).

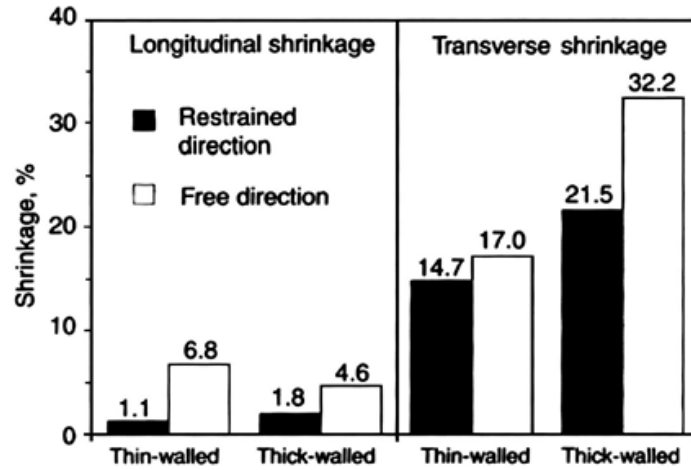


Figure 2.6: Total drying shrinkage of entire fibers, (taken from [15]).

For the wall thickness values, we find the best distribution fit (Figure 2.7). By using the parameter of this distribution, we generated numbers for each fiber and multiply it with the diameter to find the wall thickness.

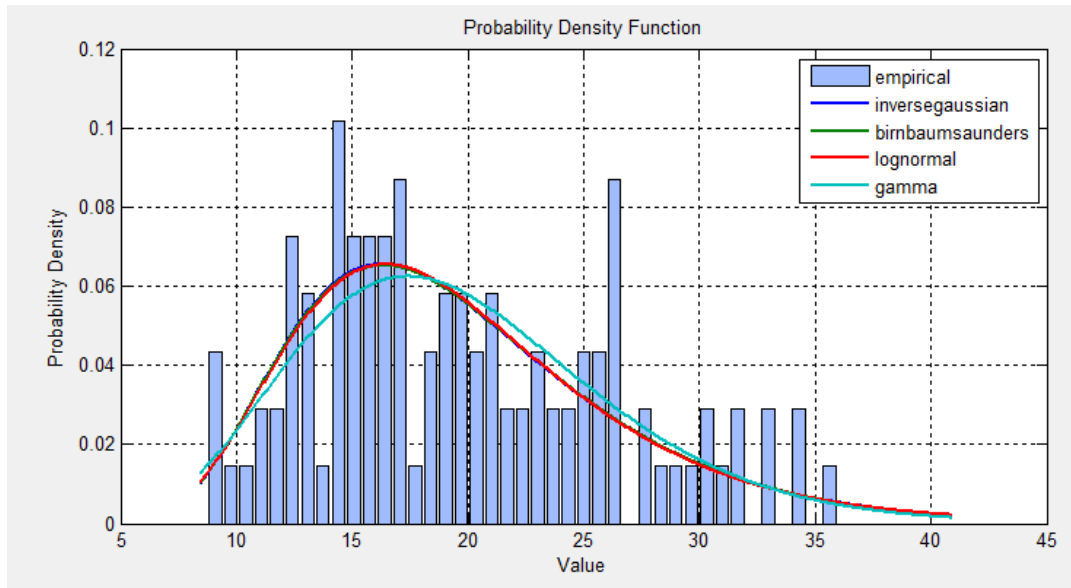


Figure 2.7: Best distribution fit from Matlab tool.

2.3 AFM test

AFM tests were used to compare the surface adhesion force with and without a presence of dry strength additives. The representative figure of the measurement is shown in Figure 2.8.

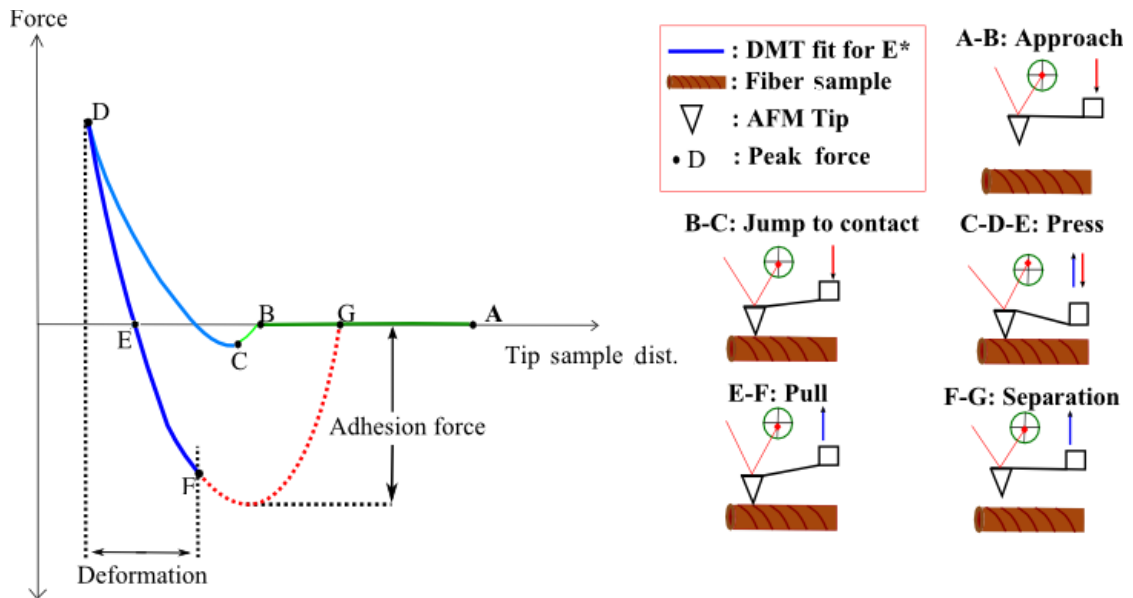


Figure 2.8: Demonstration of AFM measurement process.

In this measurement, the DMT (Derjaguin-Muller-Toporov) model was used to estimate the contact modulus. The contact modulus E^* was calculated by fitting the navy blue curve in Figure 2.8 with Eq. 2.1,

$$F - F_{adh} = \frac{4}{3} E^* \sqrt{R(d - d_0)^3} \quad (2.1)$$

where $F - F_{adh}$ is the force on the AFM cantilever corresponding to the adhesion force, R is the radius of tip end, and $d - d_0$ is the deformation of the fiber. The test results are shown in the Table 2.2.

Table 2.2: AFM measurement results.

Fiber Type	RMS Roughness (nm)	DMT modulus (GPa)	Dissipation (eV)	Adhesion (nN)	Deformation (nm)
Short Thin (Untreated)	9.6±4.1	3.7±1.0	240±120	8.9±2.7	0.6±0.2
Short Thin (Treated)	5.2±2.4	2.4±0.8	570±83	10.7±1.6	0.5±0.2
Long Thin(Untreated)	10.4±6.3	2.7±0.7	280±160	9.1±3.0	0.9±0.3
Long Thin(Treated)	5.8±2.1	2.3±0.8	440±240	9.3±1.8	0.5±0.2
Thick(Untreated)	9.6±4.4	4.1±1.2	200±88	9.3±1.4	0.7±0.3
Thick(Treated)	5.2±1.5	2.7±0.7	360±76	9.5±2.1	0.8±0.3

The results indicate that the greatest influence of the additives is observed in the contact modulus and dissipation energy, whereas the adhesion force was affected insignificantly. This indicates that adding the strength additives increased the compliance of the surface, which allowed for a greater amount of energy before the bond failure. The exact mechanisms, through which the change took place, remained unknown. One alternative is increased compliance of the fiber wall, and another one is modified surface properties [16]. The AFM principles do not allow for the direct observation of source of the deformation.

2.4 Tensile Test

The purpose of this experiment was to determine a number of handsheet paper properties, including tensile strength, strain at break, tensile stiffness, grammage and thickness. Hand-sheets with and without strength additive were provided by StoraEnso. We performed the tests in *Innventia Research Center Laboratory*.

2.4.1 Materials

We had received circular handsheet samples with radius of 8 cm. The thickness and grammage were measured for 5 handsheet samples in *Innventia Research Center Laboratory* by STFI Thickness Tester M201.

The tensile test was performed on one of the samples in *Innventia Research Center Laboratory* by using Frank Tensile Tester horizontal 81502 with *Tensile Test ISO 1924-2* test standard.

2.4.2 Methods

We divided a handsheet in 7 different pieces by 100 mm x 15.0 mm. We tested each piece in the tensile test machine and found maximum, minimum and average of maximum tensile strength and strain to failure for these seven measurements.

2.4.3 Results

Table 2.3: Samples with additive.

Sample Numbers	3	4	5	10	15
Thickness Mean(μm) \pm Std (μm)	490.9 \pm 32.8	494.6 \pm 48.0	493.7.2 \pm 52.1	535.2 \pm 50.4	493.7 \pm 52.1
Weight (g)	3.097	3.095	3.094	3.097	3.023
Radius of sample (m)	0.08	0.08	0.08	0.08	0.08
Grammage (g/m^2)	154.0	153.9	153.9	154.0	150.4
Density (kg/m^3)	313.7	311.2	311.7	287.7	304.6

Table 2.4: Samples without additive.

Sample Numbers	2	3	10	11	12
Thickness Mean(μm) \pm Std (μm)	406*	470.8 \pm 11.9	470.2 \pm 15.0	467.0 \pm 17.5	465.5 \pm 19.5
Weight (g)	3.09	3.07	3.08	3.07	3.10
Radius of sample (m)	0.08	0.08	0.08	0.08	0.08
Grammage (g/m^2)	153.8	152.8	153.3	152.8	154.3
Density (kg/m^3)	-	324.6	326.0	327.2	331.5

* The thickness measurement in one of the sample marked unusually low thickness, which was probably due to malfunction of the instrument.

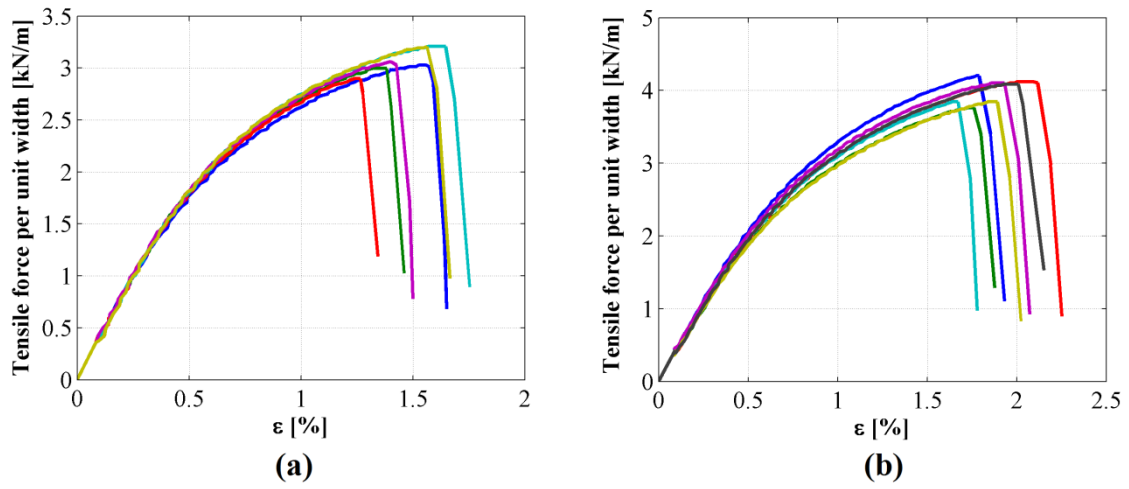


Figure 2.9: Tensile load-strain curves from different test pieces of the paper a) without additive b) with additive.

We calculated the average from all the measured curves (Figure 2.10).

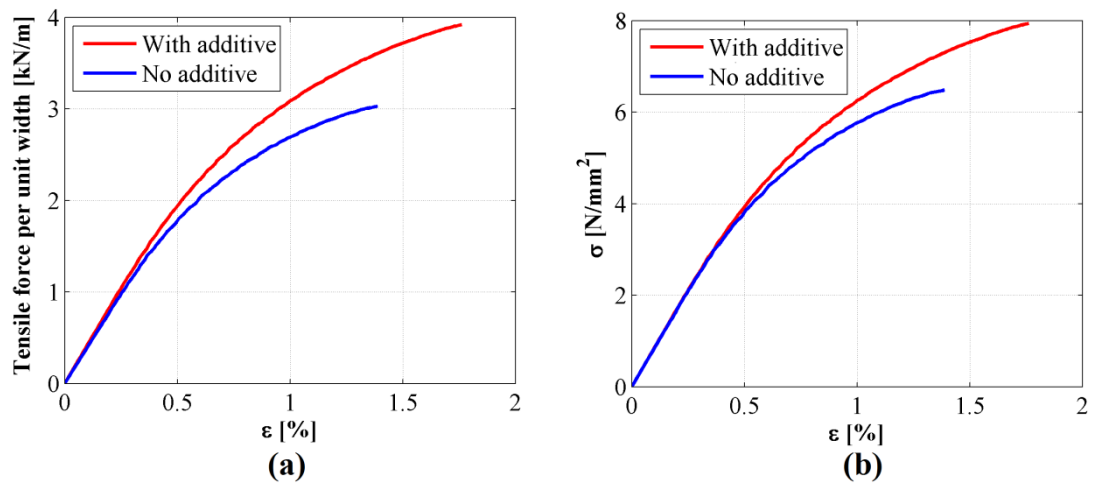


Figure 2.10: Comparison of mean a) tensile load-strain curve b) stress-strain curves.

Similar information is presented through the following diagram (Figure 2.11).

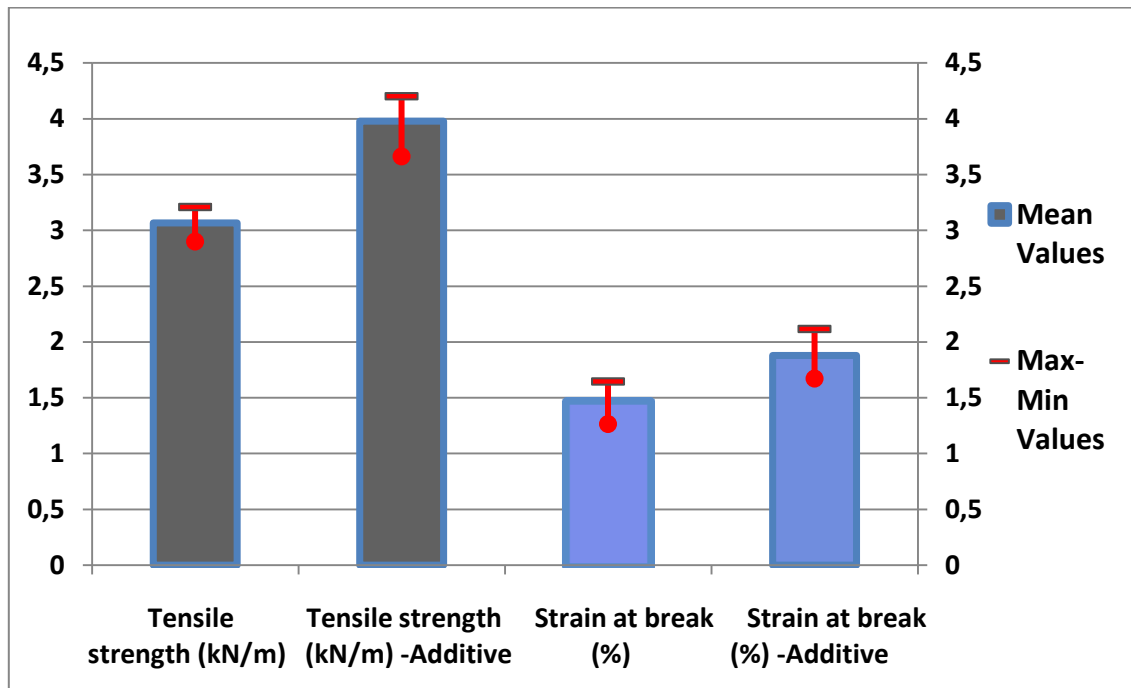


Figure 2.11: Diagram comparison of mean strength values

Figure 2.12 shows the fracture lines in the tested pieces of a sample.

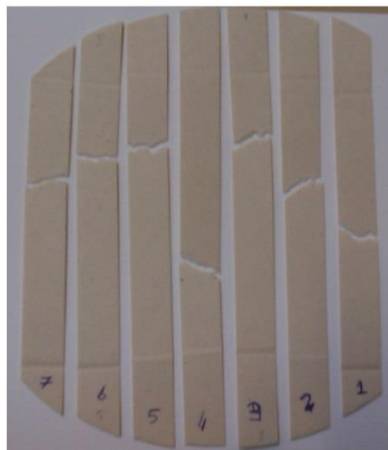


Figure 2.12: Tested and fractured tested pieces.

2.4.4 Observations

The results show that the strength additive has a fairly large impact on the parameters, tensile strength, tensile stiffness and the strain at break. The achieved improvement was 30% in tensile strength, 15% in strain at break and 5% in tensile stiffness.

An important observation is that the samples with added strength additives had considerably rougher surface. This is reflected in 3-5 times larger standard deviation in thickness measurements as compared to the sample without additive.

2.5 Digital Speckle Photography (DSP)

In this experiment, we retrieved the information about the local in-plane strains in paper while it is subjected to tensile loading. The measurement was performed with KTH - Fibre and Polymer Technology lab. The 50mm x 15mm handsheet sample was used. Detailed measurement procedures are described per Appendix. Figure 2.13 shows the recorded stress-strain curve from tensile test and the points on the curve correspond to specific instants where the strain field measurement was output and presented in Figure 2.14.

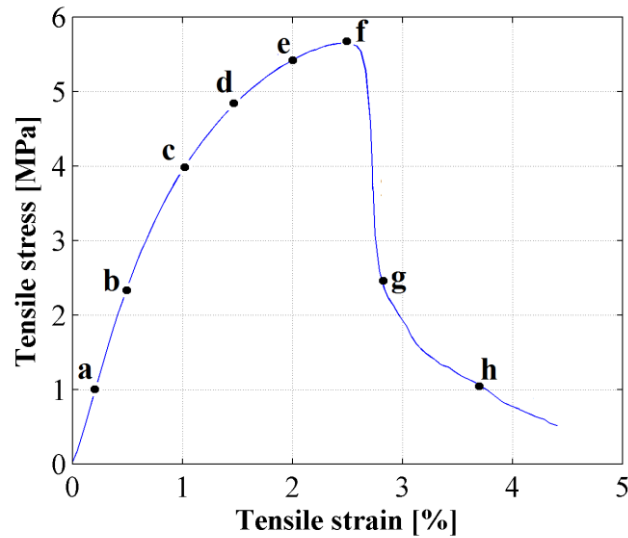


Figure 2.13: Tensile stress-strain curve.

In Figure 2.14, the strain fields measurements are given with maximum and minimum local strain values which are represented with red and magenta respectively. By comparing the maximum value of the local strain with the corresponding strain value on the stress-strain curve (Figure 2.13), we concluded that there is no significant localization prior to rupture as the maximum local strain value (3%) was fairly close to the globally recorded strain (2.6%). This can be explained by the fact that the used fibers are relatively short and have rather low number of contacts per fiber. This means that they have no potential to develop the large localization during the pull-out.

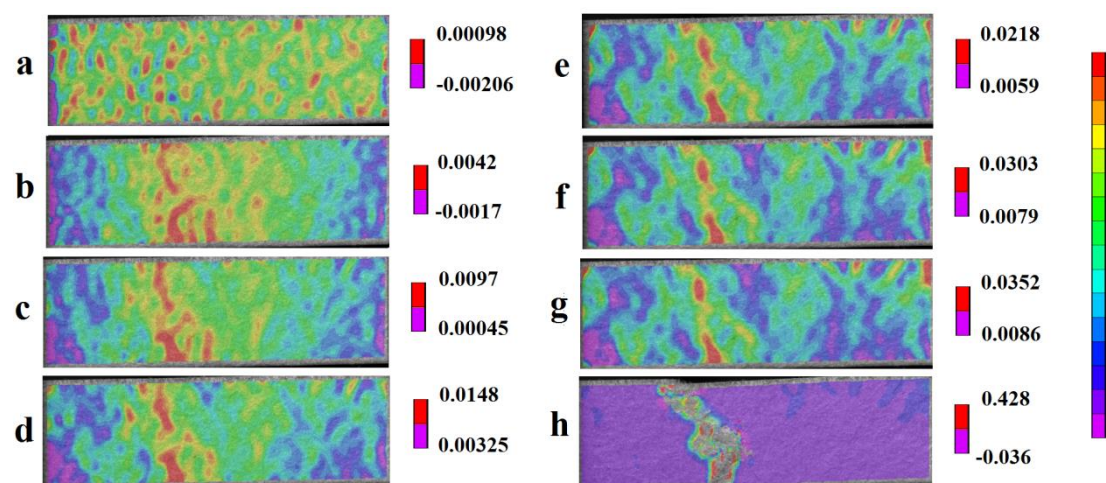


Figure 2.14: Digital speckle photography results.

Part 3

FE Fiber bond simulation

In the computational experiments, we use two different reference models. We created the first model based on the following source [17]. We use this model for the parametric study. The second model was based on the results obtained from the SEM image analyses of the paper sample. The later results were used to assign the bond stiffness parameters of the fiber network simulation. In the finite element simulations of the fiber bond, we used non-linear finite element codes with ANSYS.

3.1 Problem definition

The stiffness of two bonded fibers is a slope of the force-displacement curve extracted from the bond region under different loading conditions. In the computations, we distinguish two main component of the bond stiffness: normal and tangential. It is important to extract the data from the bond region only, avoiding the contribution from the neighboring regions. Figure 3.1 shows schematically the computational setup.

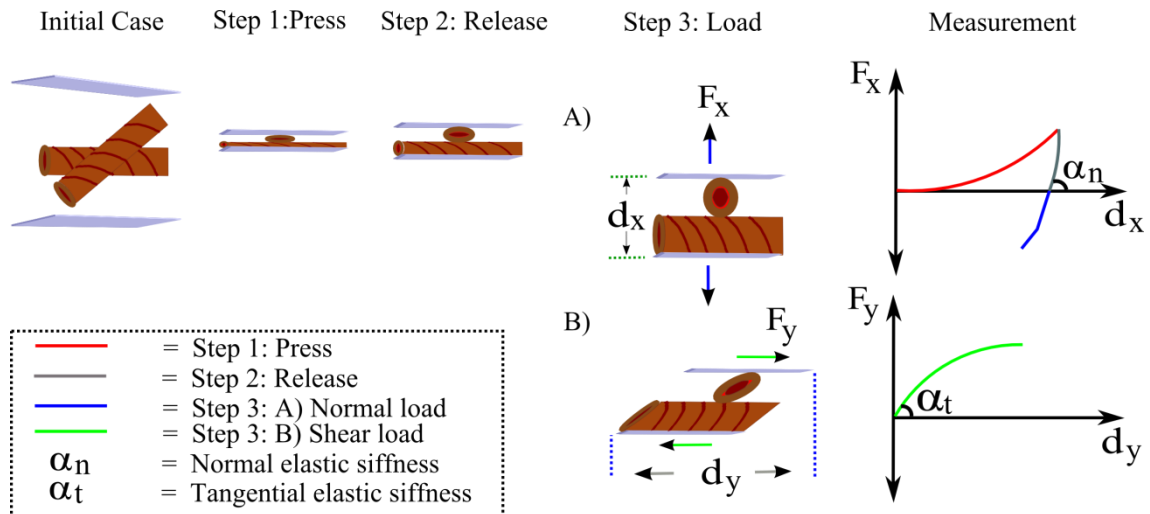


Figure 3.1: Demonstration of the bond stiffness measurement.

Two initially unstressed crossing fibers are placed on top of each other. We first press them together with rigid surfaces. During pressing, we assume that bond over the established contact areas. They are also bonded to the pressing plate. After pressing, we perform the retraction until we reach zero normal force. To compute the normal stiffness, we then continue loading in the normal direction. In shear test, we move the surfaces in the tangent direction. The parts of the fibers connected to the rigid plate are not deforming, therefore, we can reckon that the deformation take place at the contact region. The normal and tangent stiffness is computed as the slopes of the corresponding force-displacement curves.

The obtained values are to be used in the network model. In the network model, the fibers are represented as beam. The classical beam theory assumes that the cross-section of the fiber is rigid against local normal forces. The finite elasticity at the bond regions is therefore captured with contact stiffness in contact penalty algorithm. Figure 3.2 shows schematically how the stiffness values are adopted in the finite element model.

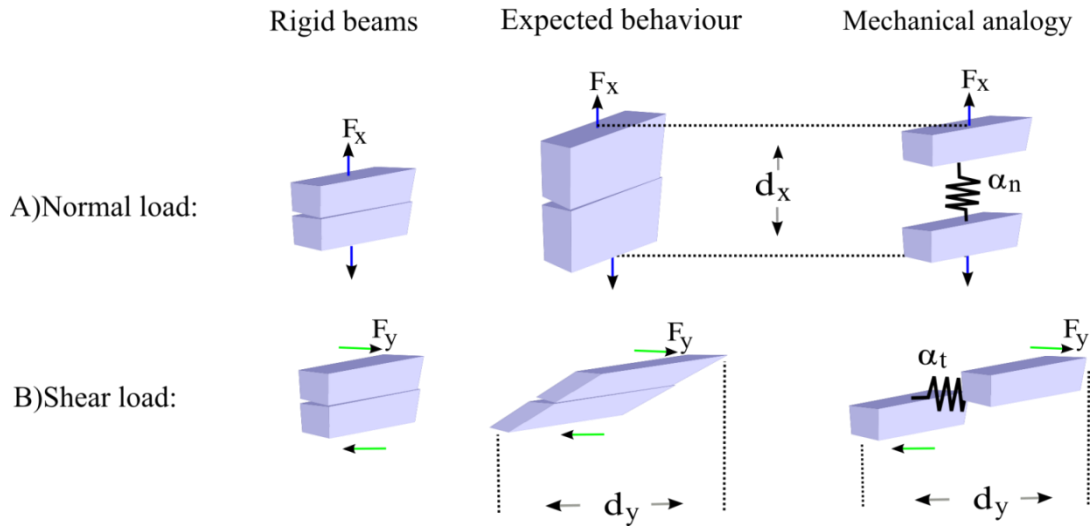


Figure 3.2: Mechanical analogy of the fibers in the network.

The thickness stretch and the tangent deformation of the bond region are represented with equivalent contact stiffness in each of the direction.

3.2 Geometry

We are going to use a 3D FE model of the fibers. In Figure 3.3, we show both SEM image and FE model of the fiber.

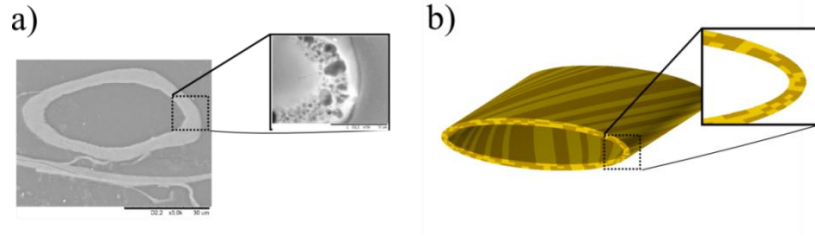


Figure 3.3: a) SEM image of the fiber cross section b) FE model of the fiber.

We consider the helical orientation of microfibrils with a specified microfibril orientation angle MFA as shown in Figure 3.4.

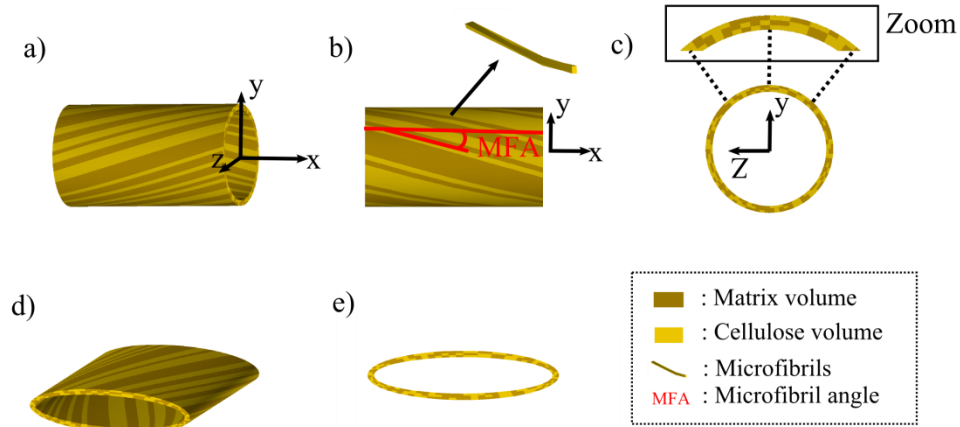


Figure 3.4: FE fiber model.

To be able to mimic partly collapsed fibers, we assume elliptical shape for the fiber cross-section (see Figure 3.4). Figure 3.5 shows the two reference models where MFA is 16 degrees and length of the fibers is assigned $5\mu\text{m}$ more than fiber width. In the computations we assumed that both the fibers in the bond region have identical geometries.

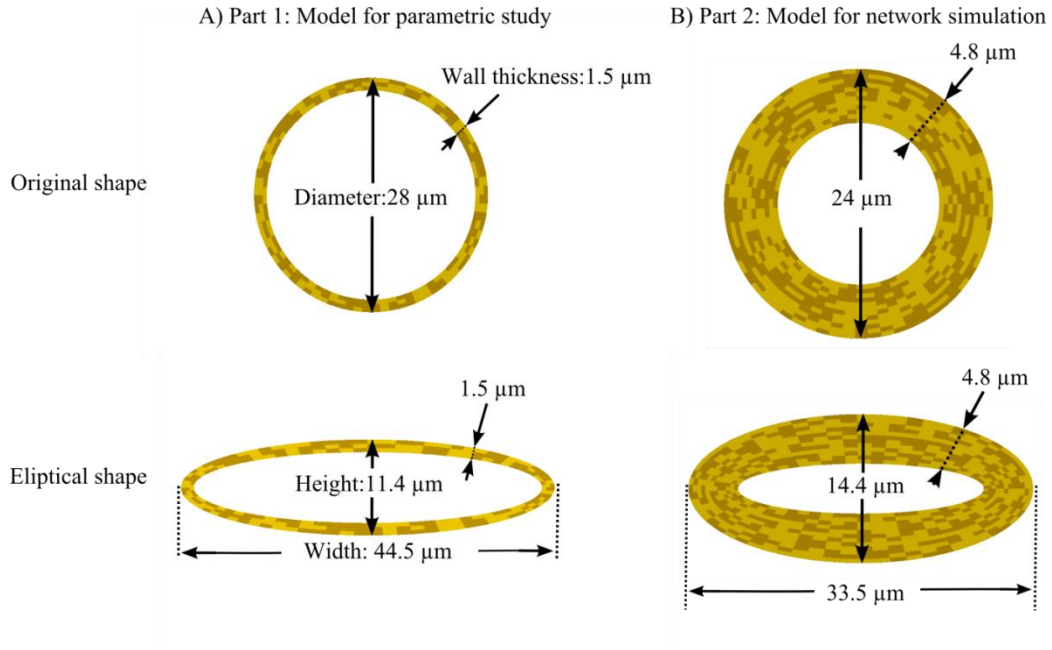


Figure 3.5: FE fiber dimensions a) based on [16] and b) based on SEM results.

3.3 Material

We selected the material parameters for the cellulose microfibril and the surrounding matrix based on the following references [16] and [17], which are listed in Table 3.1. The cellulose microfibril material is assumed as linear orthotropic, and the matrix material is linear orthotropic until yield. After reaching the yield stress of 220 MPa, it is assumed to exhibit elastic-ideally plastic behavior.

Table 3.1: Material parameters of FE model.

	Cellulose microfibril	Matrix material
Ezz [GPa]	134	8
Exx [GPa]	27.2	4
Eyy [GPa]	27.2	4
Gxy [GPa]	13.1	2
Gxz [GPa]	4.4	2
Gyz [GPa]	4.4	2
ν_{xy} [GPa]	0.04	0.01
ν_{xz} [GPa]	0.1	0.2
ν_{yz} [GPa]	0.1	0.2
Volume fraction	45	55

3.4 Mesh

We used 8 node solid elements for meshing the fibers. We performed the mesh convergence study for the used geometries. To be able to find the optimum mesh size we started with an initial coarse mesh by selecting a division factor n as one and increased until we reached the converged values (see Figure 3.6).

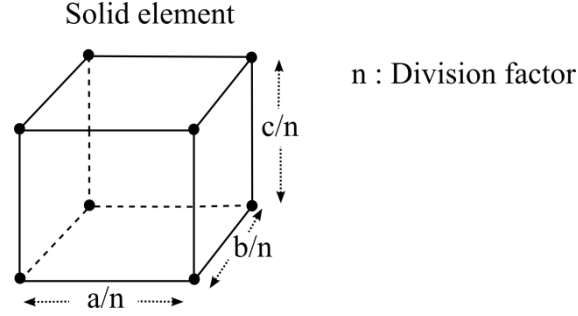


Figure 3.6: 8 nodes solid element.

Once we reached the converged mesh size, we started to decrease the division factor in each direction to obtain the optimum mesh and yet to ensure the computation efficiency.

For the first reference geometry, we used initial a , b and c solid element dimension values as $4.5\mu\text{m}$, $3\mu\text{m}$ and $1.5\mu\text{m}$ respectively. In Figure 3.6 we divided solid element dimensions by from 1 to 5 for each simulation and found the stiffness values. After division number 4, the stiffness deviation was less than 0.05% which was considered sufficiently low (see Figure 3.7).

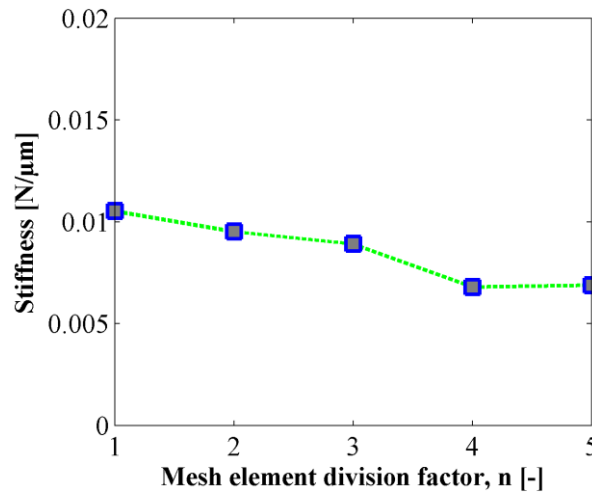


Figure 3.7: Stiffness values for different mesh sizes.

After we found the optimum division value, we divided each dimension of solid element individually by from 1 to 4 while we kept the other dimensions same for each

simulation and found the stiffness values. As it is shown Figure 3.8a, for dimension a we reached the optimum stiffness value at division number 4. For the other two divisions, b and c we reached the optimum stiffness at 3 for both (see Figure 3.8b, c).

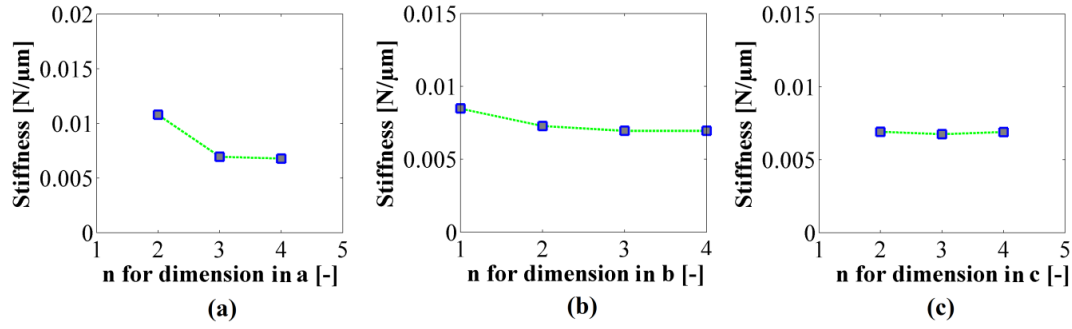


Figure 3.8: Stiffness values against different mesh sizes in individual dimensions.

With the optimum mesh, each simulation took about 15 hours on a 4x2.67 GHz machine. Similar procedure was repeated for the second reference geometry. Figure 3.9 and Figure 3.10 show the optimal mesh for the both reference geometries.

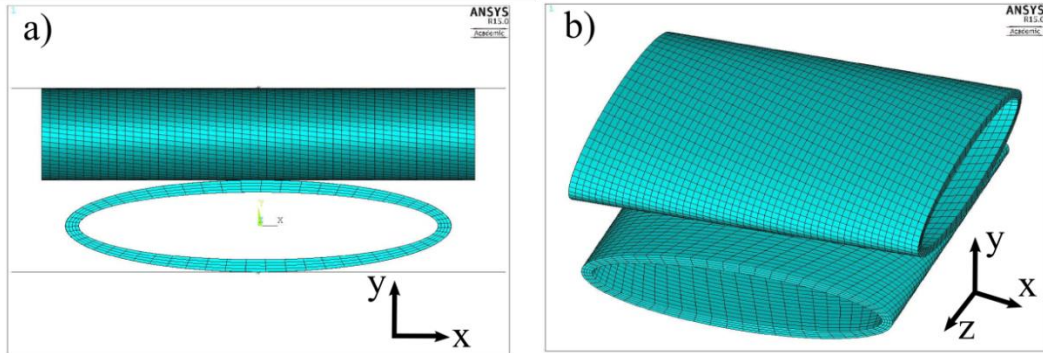


Figure 3.9: Meshed body of the first geometry.

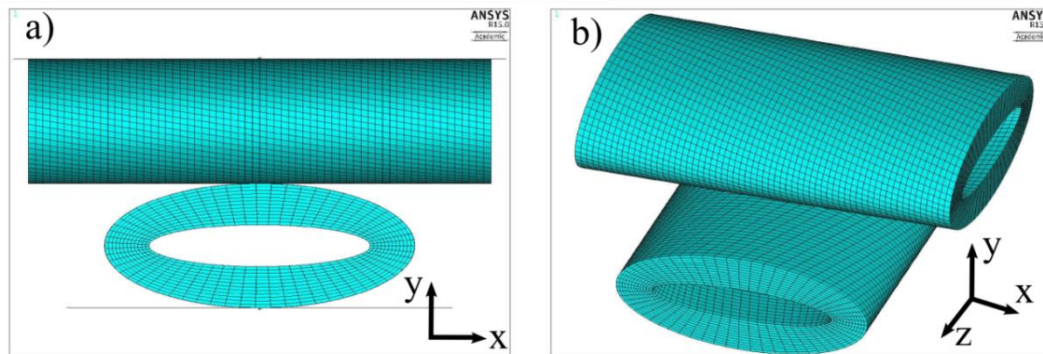


Figure 3.10: Meshed body of the second geometry.

3.5 Boundary conditions

Setting appropriate boundary conditions is vital for ensuring that the recorded response is computed from the bond region. At the same time, the fibers have to be constrained to prevent undesired rigid body motion. One end of the fiber was constrained entirely in the longitudinal direction. All the nodes on the other end formed a coupled set in the longitudinal direction, which prevented rotations but yet allowed fiber to deform in the longitudinal direction. Therefore, the fraction of the elastic energy stored in the longitudinal mode was insignificant. Figure 3.11 shows the specified constraints.

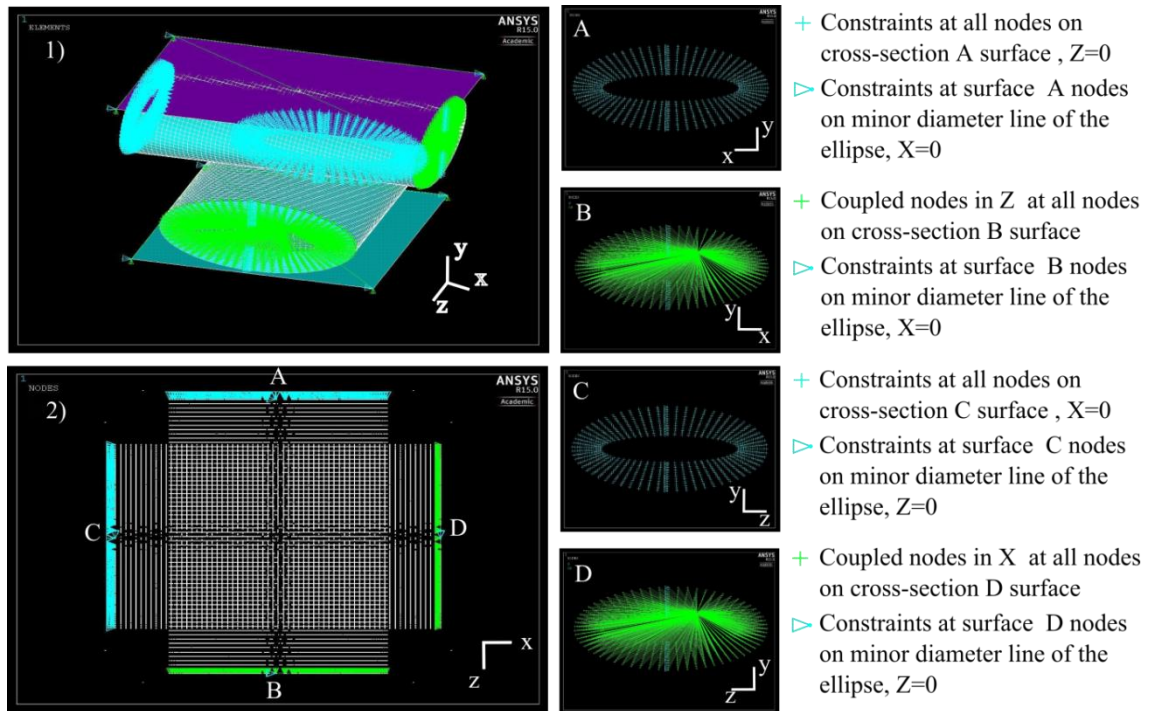


Figure 3.11: Constrains of the fiber bond model.

3.6 Computational experiment

Using the model, we performed a series of parametric studies with the goal studying the effect of relative bonded area (RBA), wall thickness, contact angle, diameter, MFA, fiber shape, maximum applied press and inner contact.

In Figure 3.12, we show the deformed state of the fiber bonds from different load steps. The results of the test are presented as force-displacement curves. We fitted a 3rd order polynomial to find the slope (i.e. the bond stiffness) around unstressed state. In the reference model we pressed the bond to the 95% of inner space between fiber walls

(fiber minor diameter- 2*wall thickness). The reason of selecting 95% is bringing the inner surfaces of the fibers in “just-in-touch” position. We studied however the effect of pressure as one of the variable in the parametric study.

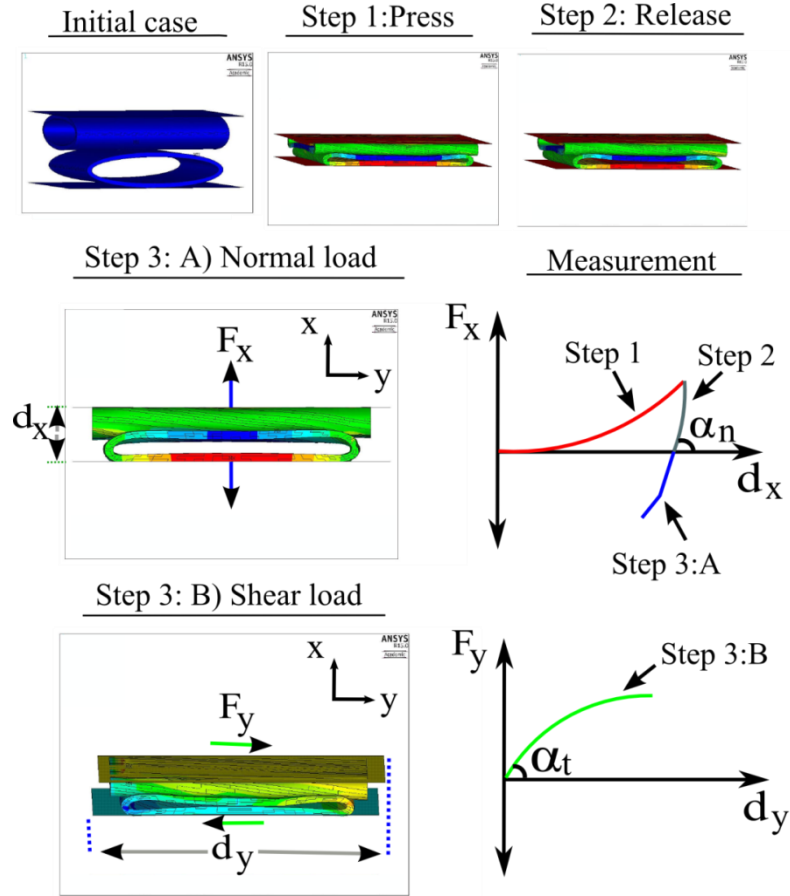


Figure 3.12: Demonstration of the bond stiffness measurement in the simulation.

3.7 Results

Part 1: Parametric study

Normal and shear load

Figure 3.13 shows a typical force-displacement response in the normal and tangent direction.

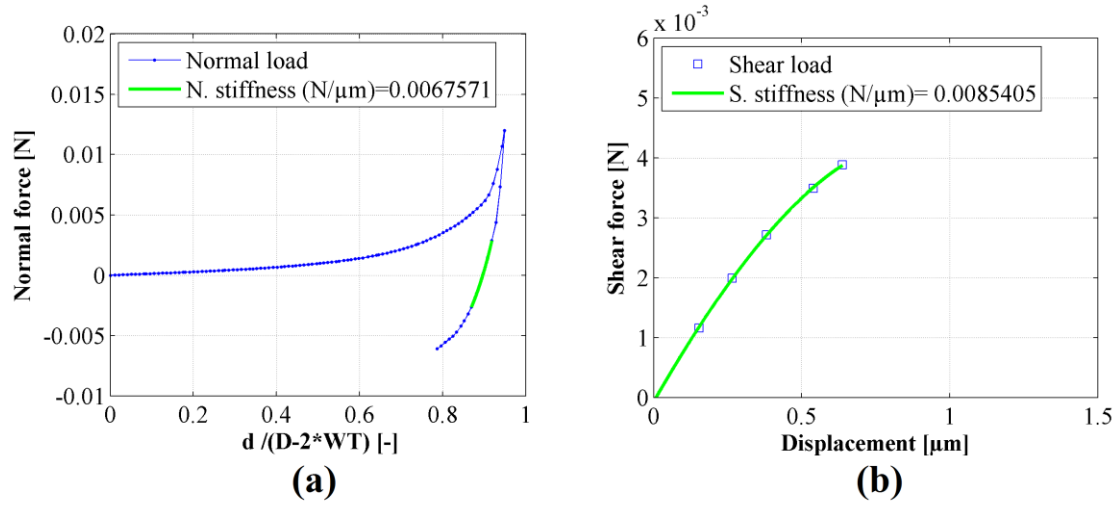


Figure 3.13: Force displacement curve of a) normal load b) shear load.

The normal response exhibits the stiffening as the fibers' inner surfaces are brought into contact and the response is driven by the compression of the wall itself. The shear response is recorded once the fibers are pressed and unloaded. The green line shows the third-order polynomial fitted to the response curve and used to estimate the slope of the curve, which we refer to as contact normal and tangent stiffness.

Diameter

We change the diameter of the fibers in this part by keeping the same wall thickness to see the effect of the diameter. Figure 3.14 shows that with a given wall thickness, the diameter has surprisingly limited effect on the shear and normal contact stiffness.

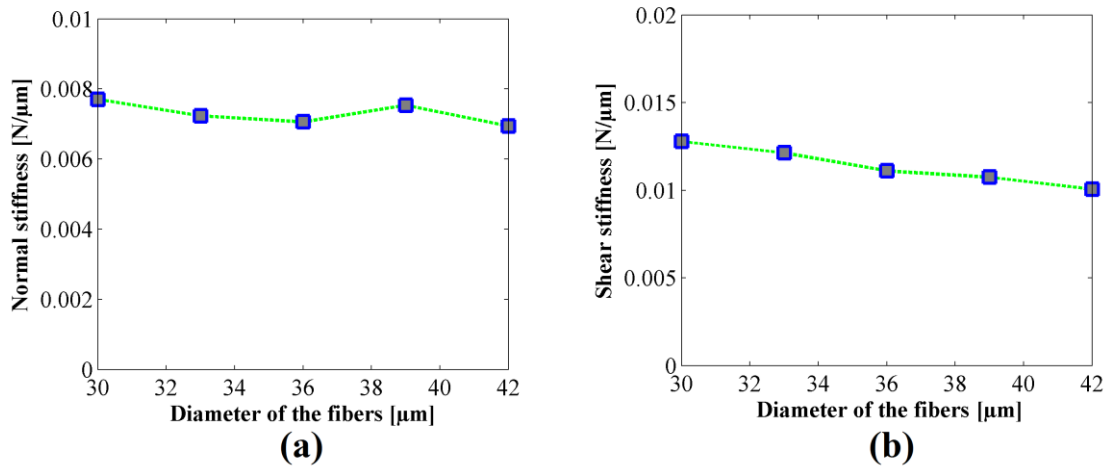


Figure 3.14: Comparison of the stiffness for the different diameter cases.

Contact angle of two fibers

We tested the different crossing angles where we also changed the shear load direction while we kept the below fiber in the same position (see Figure 3.15). In the other models, we always used 90 degree cross angle for other models.

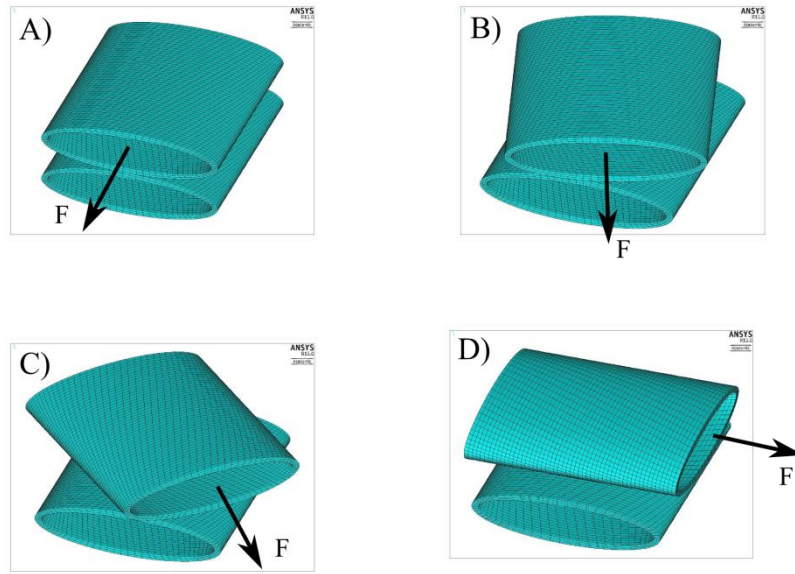


Figure 3.15: Different contact angles a) 0 b) 15 c) 45 d) 90 degree.

Figure 3.16 and 3.17 shows the stiffness change for different contact angles.

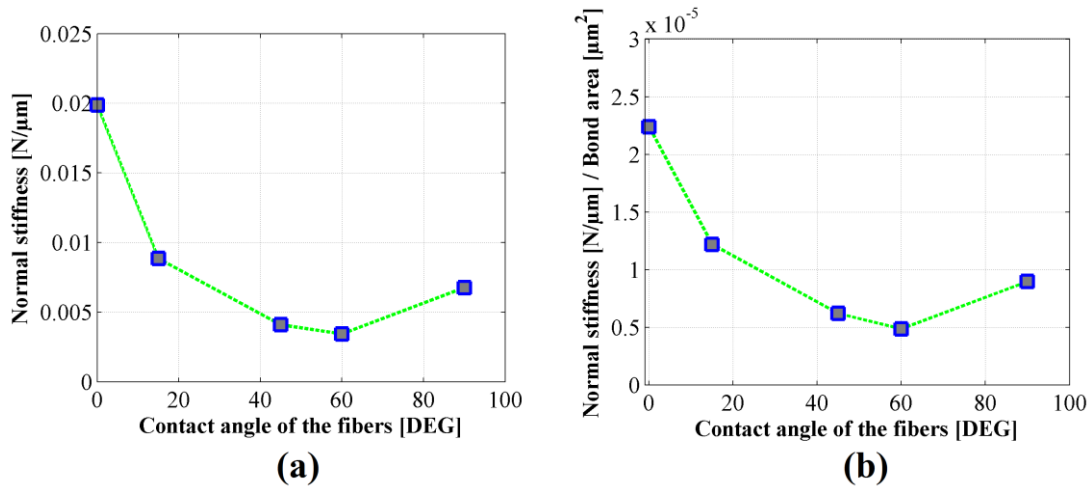


Figure 3.16: a) Comparison of the normal stiffness for the different contact angle cases b) stiffness normalized with overlap area.

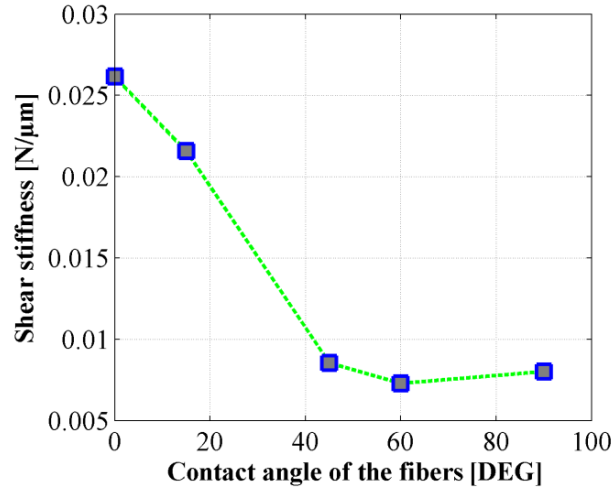


Figure 3.17: Comparison of the shear stiffness for the different contact angle cases.

There are two important observations to be done from these figures. First, the normal and shear contact stiffness are dependent on the bond geometry. For examples, it reaches the minimum value at 60 degree orientation with the fibers having 16 degree MFA. Another important observation is that this dependency is not due to changes in the overlap area.

Initial shape

Many fibers are initially collapsed. In other words, the cross-section of the fiber is not circular. Figure 3.18 shows the different initial fiber shapes that we simulated the bond stiffness for these cases in 3.19.

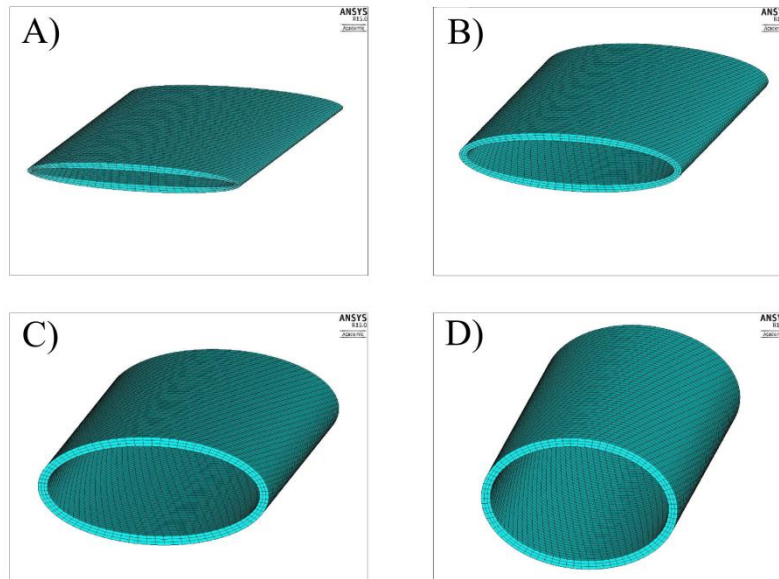


Figure 3.18: Initial collapsed shapes for a/b ratio as a) 8/48 b) 12/45 c) 18/38 d) 23/33

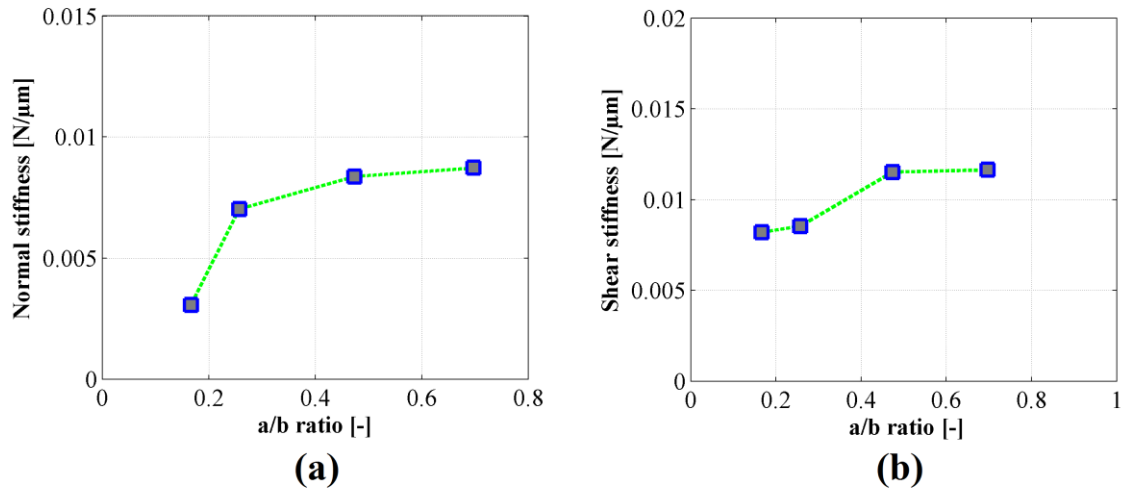


Figure 3.19: Comparison of the stiffness for different ratios between minor and major diameters of the elliptical cross-section.

Wall thickness

The greater the wall thickness is the larger the force should be applied to press the fibers (Figure 3.20a). At a given degree of compression and the diameter, the stiffness changes almost linearly with the wall thickness at Figure 3.20b and 3.21b.

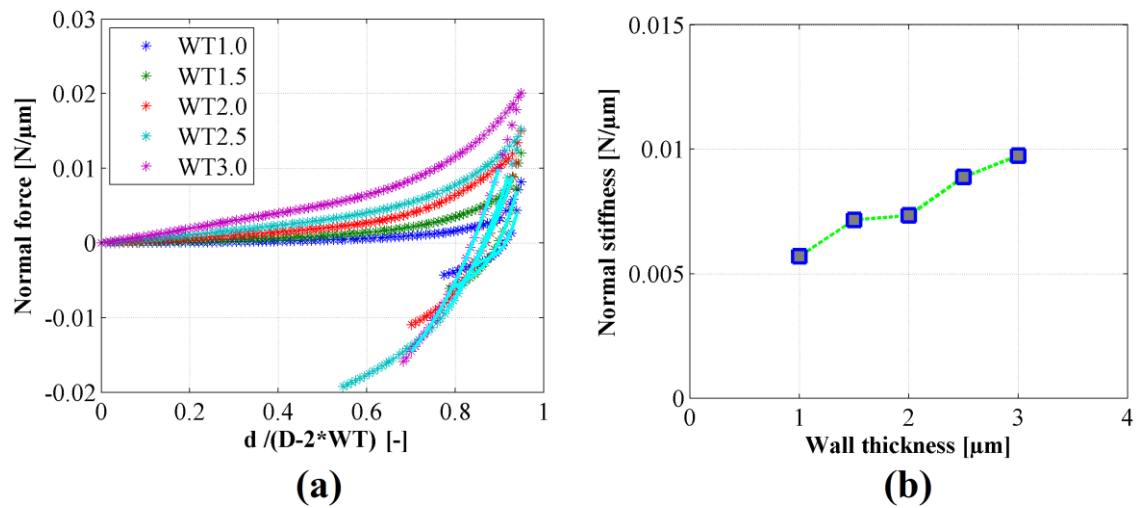


Figure 3.20: a) Normal force-displacement curve for different wall thicknesses b) normal stiffness as a function of the wall thickness.

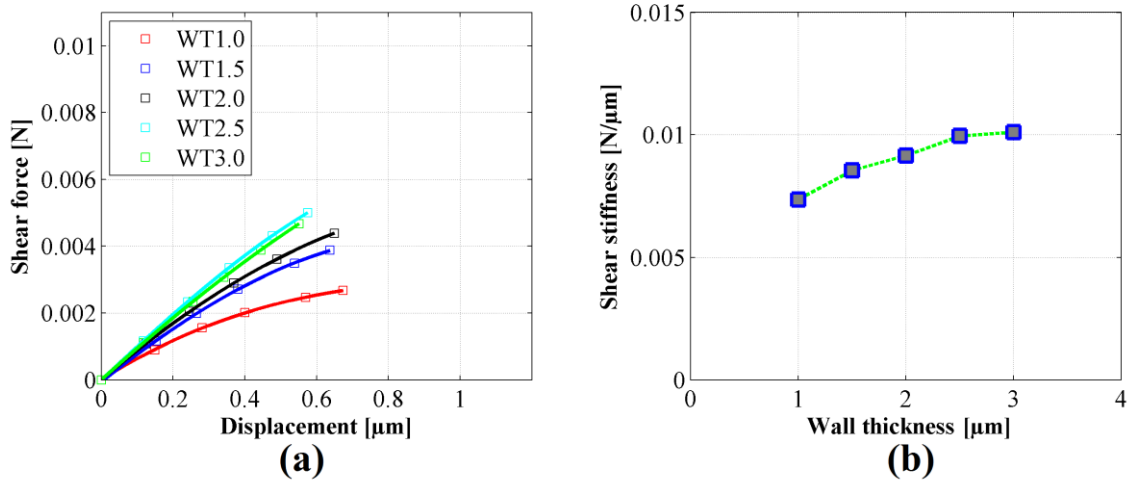


Figure 3.21: a) Shear force-displacement curve for different wall thicknesses b) shear stiffness as a function of the wall thickness.

Effect of the inner contact

As the fibers are pressed the, the inner surface may establish the contact and stay closed. The effect of this was tested by forcing the bonded self-contact onto the inner surface. This means that the surface does stay closed. Figure 3.22 and 3.23 show that the presence of the bonded inner contact expectedly increases the normal stiffness by a factor of 4, which is not a desirable effect with respect to the separation energy of the bond, which can be significantly decreased due to it.

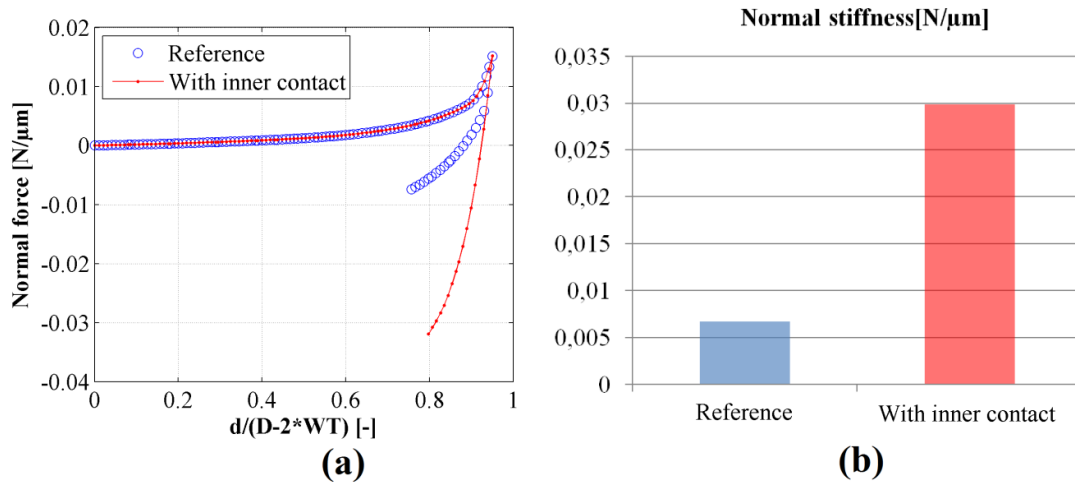


Figure 3.22: a) Normal force - displacement curve of different normal and inner bonded fibers b) comparison of the normal stiffness for normal and inner bonded fibers.

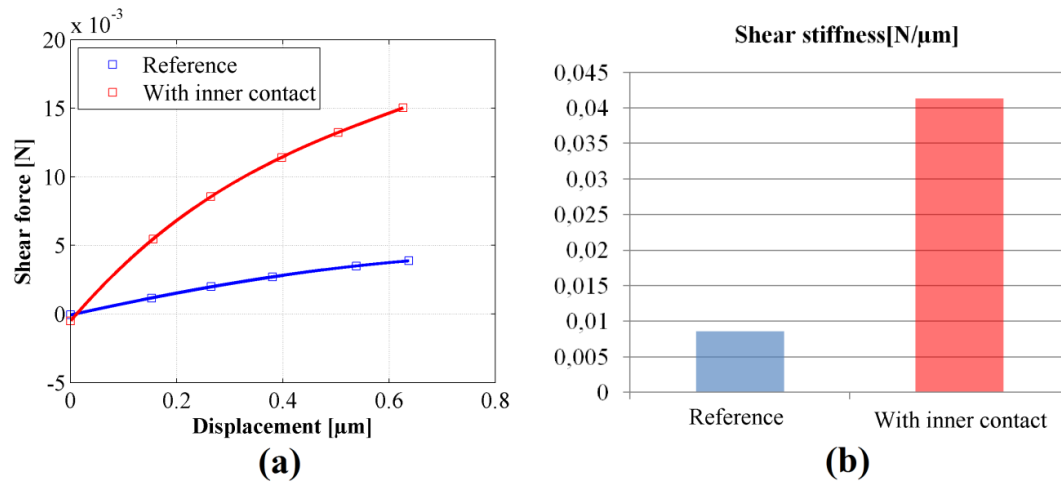


Figure 3.23: a) Shear force displacement curve of different shear and inner bonded fibers b) comparison of the shear stiffness for normal and inner bonded fibers.

Part 2: Model for network simulation

In this part MFA was selected as 23 degree.

Relatively bonded area (RBA)

To be able to test the effect of the fiber bond area on the stiffness, we changed the amount of the bonded contact elements between the fibers. In Figure 3.24, we assign the elements in the fiber crossed area 15%, 25%, 35% and 100% as bonded contact for each calculation.

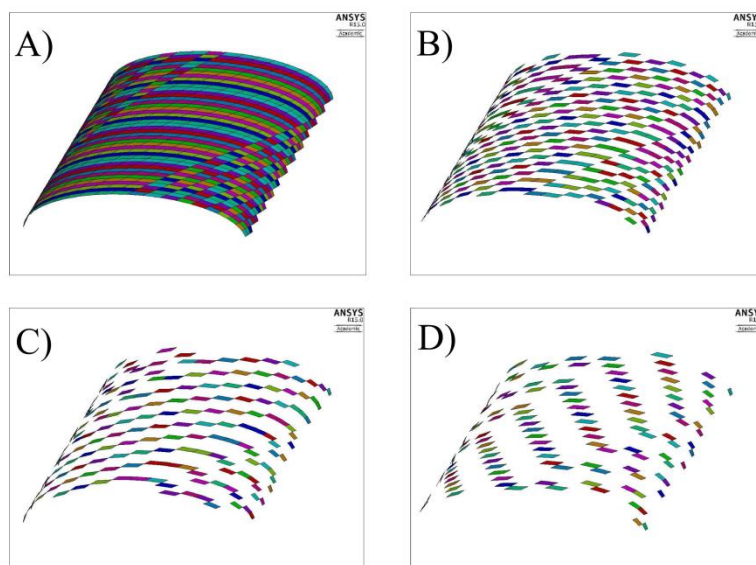


Figure 3.24: Fiber crossed surface a) 100% b) 35% c) 25% d) 15% bonded contact.

The result shows that between 35-100% there is minor effect of bond area on the stiffness, which is an expected results, since most of the deformation energy is stored in the global deformation of the fiber, that is unaffected by contact area varied in a reasonable range (see Figure 3.25). Obviously, RBA changed through the area of individual bonds will have an impact on the bond strength, but the direct relation between RBA and bond strength is outside the scope of this work as it would require enhancing the detailed bond model with debonding capabilities. We will however study the effect of RBA indirectly by varying the bond strength and the number of contacts in the network model later.

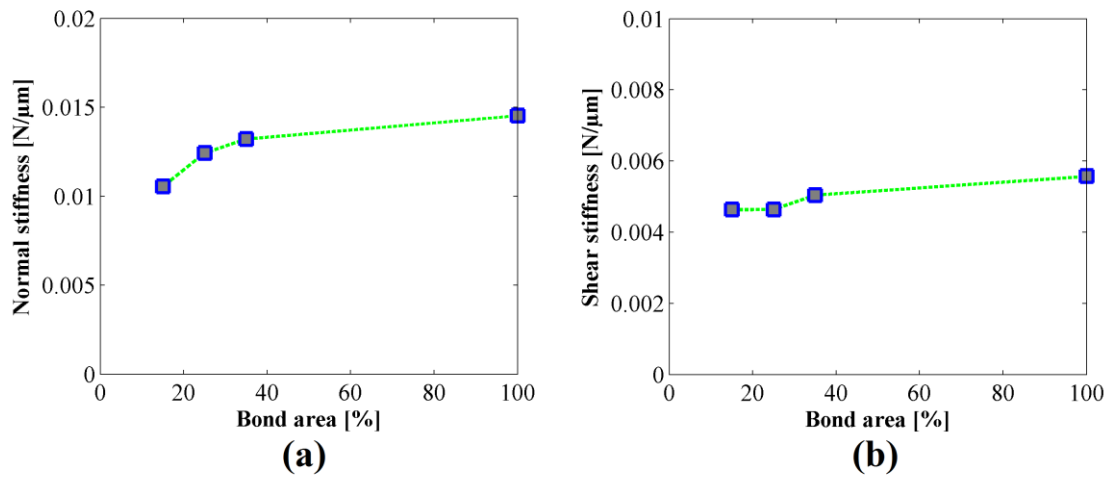


Figure 3.25: Comparison of the stiffness for the different bond area percentages.

It is worth mentioning that contact area in the bond originally has bonded and non-bonded areas, which are there purely due to non-uniform deformation in the bond region (see Figure 3.26). It resembles the appearance of the bonding areas seen by schematic representation of the contact zone in [16] (Figure 3.27).

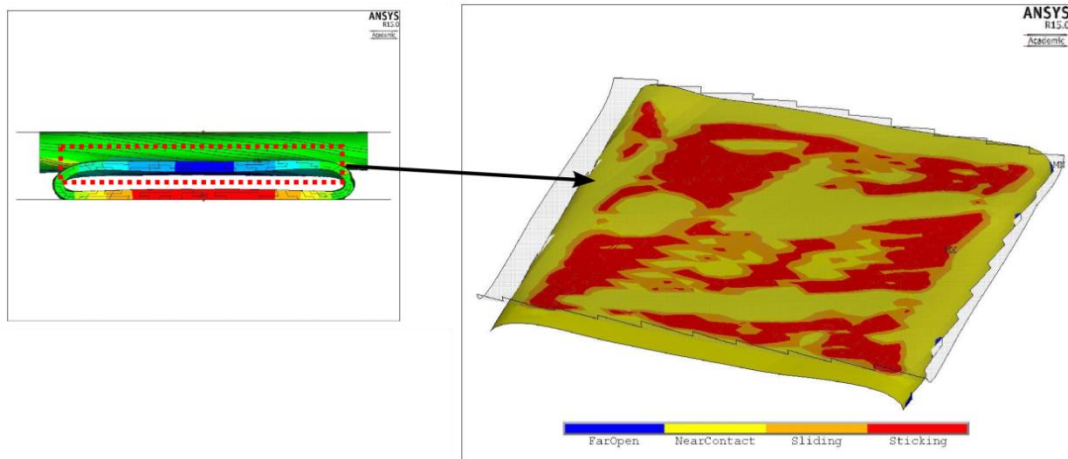


Figure 3.26: Bonding area of two fibers where red color represents the bonded area.

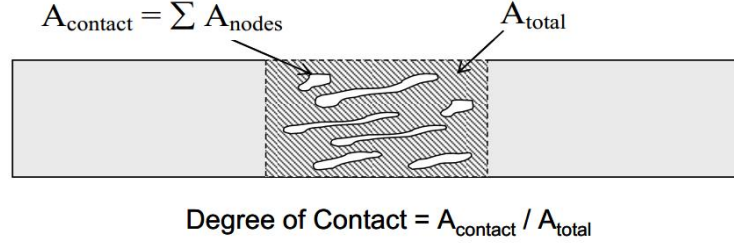


Figure 3.27: Schematic representation of the contact zone between two fibers (taken from [15]).

This shows that even with two smooth surfaces, one can hardly expect that the bonded region will cover the entire bond overlap area.

Effect of pressure

In this part we applied three different amounts of maximum press forces to see the effect on the stiffness (see Figure 3.28).

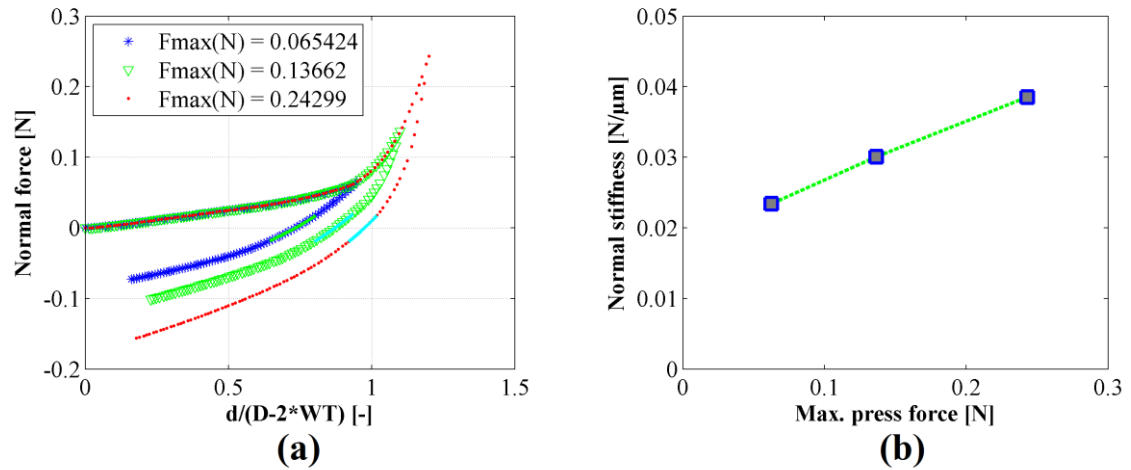


Figure 3.28: a) Normal force displacement curve of different maximum press force b) normal contact stiffness as a function of applied pressing force.

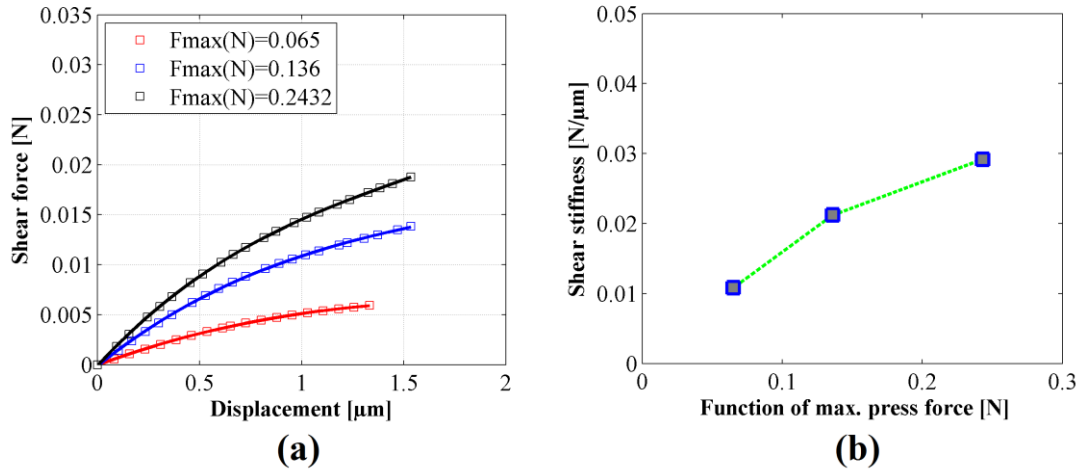


Figure 3.29: a) Shear force displacement curve of different maximum press force b) shear contact stiffness as a function of applied pressing force.

As you can see in the figure, max press force has the fairly large effect on the stiffness. This result shows that the force that we apply when we produce a paper changes the stiffness of fiber bonds and affects the strength of paper.

MFA

The effect of MFA was surprisingly not very significant compared to other factors on the normal contact stiffness. However, it has quite large impact on the shear contact stiffness. This is due to different mechanics of the deformations. MFA has apparently large impact on the shear stiffness of the fibers.

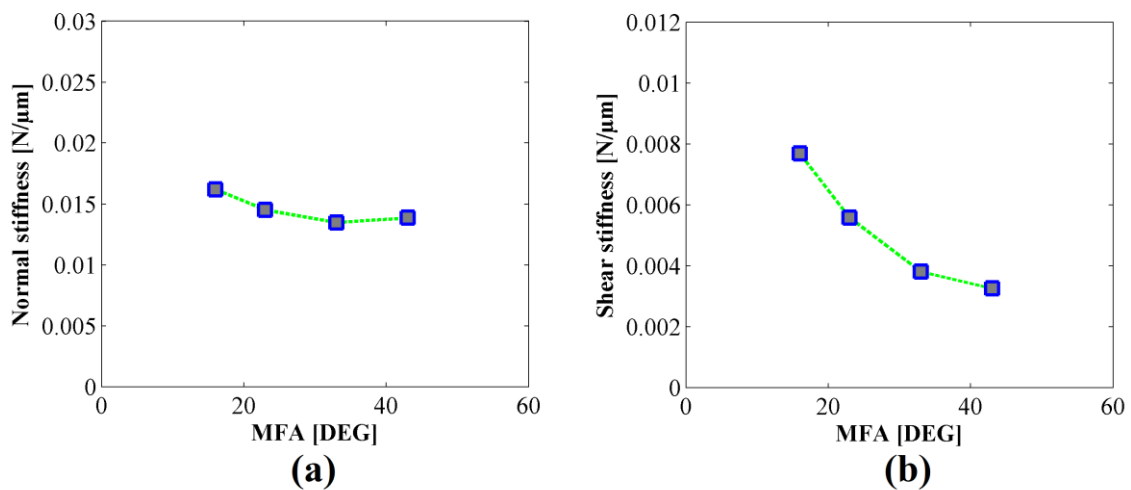


Figure 3.30: Comparison of the stiffness for MFA.

Part 4

3D Dry fiber network simulation

In this section, we are going to describe the procedure for 3D fiber network generation and implementation of this network in the FE simulation by Fibnet.

4.1 Network generation

We assign each fiber with certain length, wall thickness, diameter, curl, fiber orientation, and also crossed fiber segment's properties in transversal direction while we deposit the fibers on a flat plane. All fiber properties assigned according to the fiber characterization and SEM results as described earlier. The orientation and the position of fibers were random, which ensured isotropic fiber orientation in the plane. The grammage of the network was set to the target value to match the tested handsheets.

4.1.1 Fiber cross-section

According to the SEM image analyses, more than a half of the fibers have hollow rectangular cross section instead of circular hollow so we represented the fibers with hollow rectangular cross-section in the network (See Figure 4.1). This transformation affects the thickness of the network as well as the bending resistance of the individual fibers.

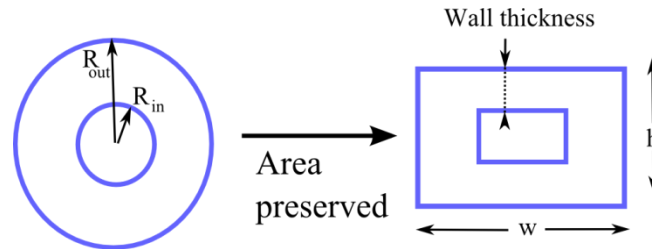


Figure 4.1: Fiber cross section modification.

When we change the cross-section of the fibers, we preserve the cross section area and the wall thickness values. By preserving these two parameters, we find width and height values for each fiber with initially assigned width/height ratio. This ratio gave us a

possibility to set the network thickness to the test paper thickness by manipulating it. We increased the ration until we reached the correct thickness.

4.1.2 Fiber curl

In the model, we represent the fibers by second order polynomial functions. Figure 4.2 demonstrates the fiber curl where L represents the real length of fiber, and C represents the projected length of fiber.

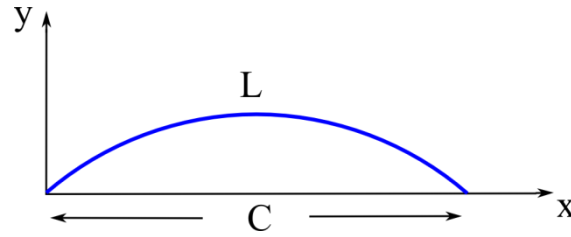


Figure 4.2: Fiber curl representation.

In the fiber characterization test, we got L and C values of the 7000 fibers from our pulp that we used to generate the test paper. By using these L and C values we express the length of curve in Eq.4.1 and fit a polynomial curves to find the function constants a in Equation 4.2.

$$L = \int_0^C \sqrt{1 + \left(\frac{dy}{dx}\right)^2} \quad (4.1)$$

$$y = a \cdot (x^2 - x) \quad (4.2)$$

Once we have a values for each fiber, we assign the fibers shape with Eq.4.2 by these constants in fiber shape generation part of the algorithm.

4.1.3 Fiber disposition

We generated randomly oriented and positioned fibers within prescribed area (see Figure 4.3). These fibers had to be deposited on the flat surface. The target area was increased by the average length of the fibers, which was than cropped to avoid boundary effects.

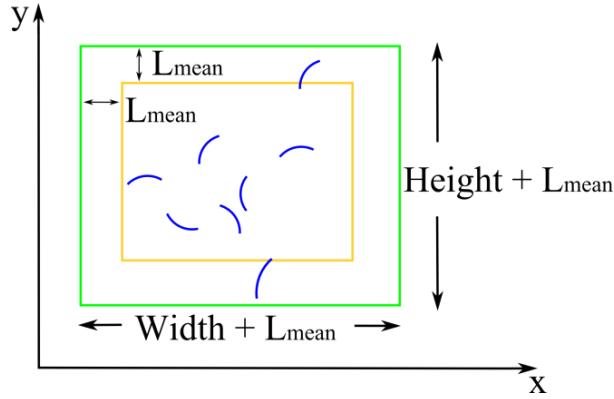


Figure 4.3: Deposited few fibers representation on 2D.

The next step was forming the 3D network by deposition technique described in the next section.

4.1.4 Fiber on 3D space

We described the each fiber as a chain of parabolic segments. The fibers land on the flat surface on by one to mimic the handsheet-making process. If there are underlying fibers already on the surface, the fiber will change shape and bend around the fibers in a way to preserve the maximum bending angle of 30 degrees. The maximum bending angle controls conformation of the fibers and one of the ways to affect the final thickness of the sheet (Figure 4.4).

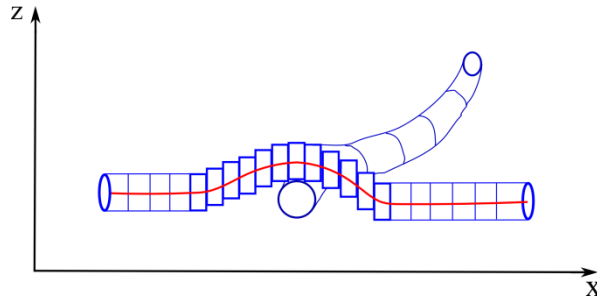


Figure 4.4: Fiber segment correction in 3D.

We repeat this process until we reach the target grammage of network. We export the network structure in the format which could be used in the Finite Element simulations later. The entire flow of events in the deposition algorithm is depicted in the diagram below.

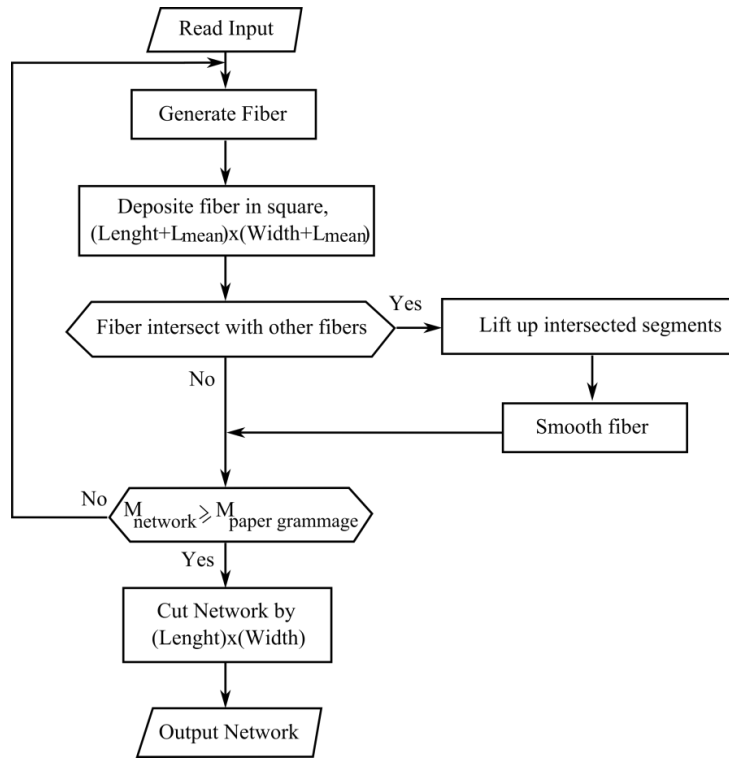


Figure 4.5: Flowchart of the 3D fiber network generation algorithm.

4.1.5 Network thickness

During the deposition, the upper surface of the network became rough and thickness varied spatially. It can be demonstrated by the density profile in the thickness direction. The density profile was expectedly non-uniform with denser network structure closer to the bottom (i.e. closer to the flat surface) and sparser network closer to the upper surface (Figure 4.6).

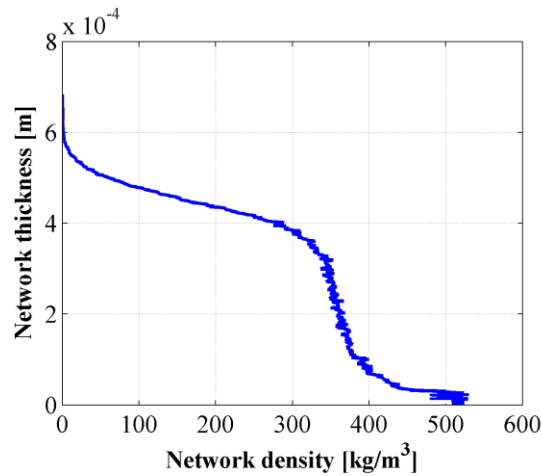


Figure 4.6: Density profile in thickness direction from the generated network in Fortran.

We measured the thickness according to center of mass of the fiber network (Eq. 4.3). Then we mirrored all the fiber segments over the center of mass (Eq. 4.4). We computed the new center of mass (Eq. 4.5) and multiply it by 4 to estimate the total network thickness (Eq. 4.6). By using this method, we accounted for non-uniformity of density profile.

$$\text{Step 1: } Network_{center\ of\ mass}(z) = \frac{\sum_n \sum_i fiber_n segment_i(z) * segment_i mass}{\sum_n fiber_n mass} \quad (4.3)$$

$$\text{Step 2: } fiber_n segment_i(z)' = |fiber_n segment_i(z) - Network_{center\ of\ mass}(z)| \quad (4.4)$$

$$\text{Step 3: } Network'_{center\ of\ mass}(z) = \frac{\sum_n \sum_i fiber_n segment_i(z)' * segment_i mass}{\sum_n fiber_n mass} \quad (4.5)$$

$$\text{Step 4: } Network\ thickness = 4 * Network'_{center\ of\ mass}(z) \quad (4.6)$$

This estimate thickness value was on average 20% percent lower than the highest point in the density profile. For the computations, we generated 10x10mm network, which is shown in Figure 4.7.

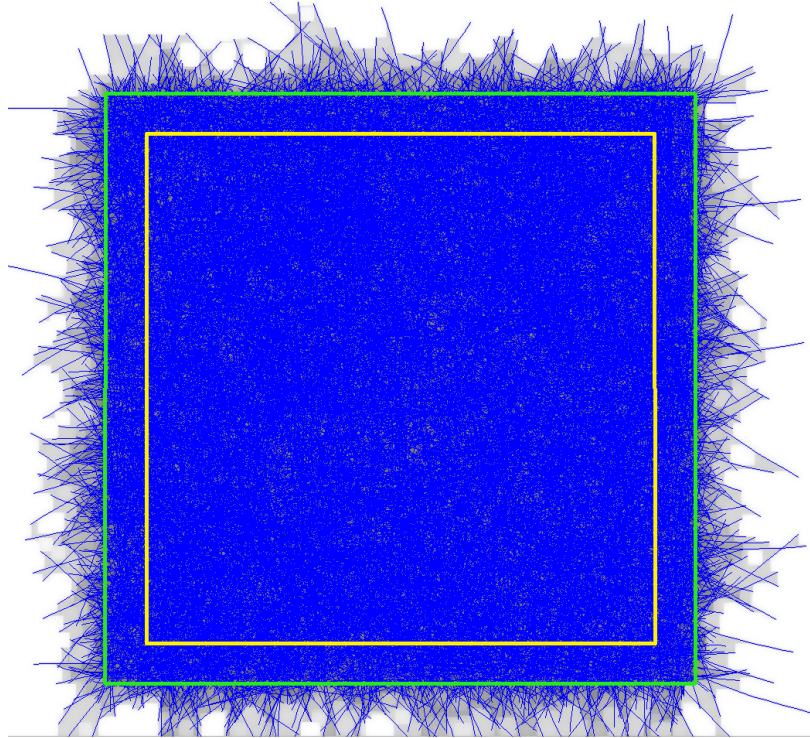


Figure 4.7: Fiber network generated by deposition technique. Green lines show the total area, yellow lines show the cropped area.

4.2 FE network model

The fiber structure is imported into finite element solver (FibNet). The solver is integrated into commercial software (ANSYS), which gives possibilities for visualization, pre- and post-processing. Figure 4.8 shows a 5x1 mm snippet of the network.

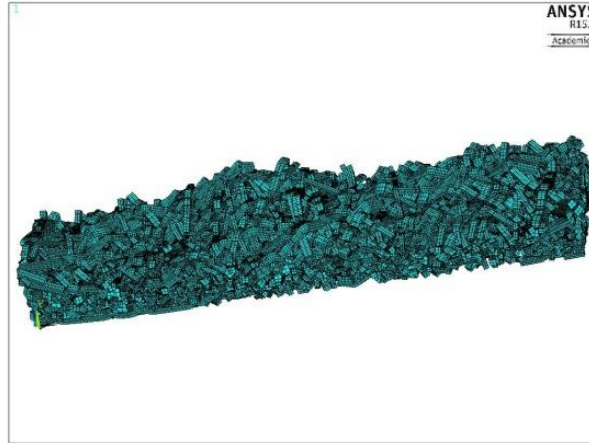


Figure 4.8: 5mm x 1 mm network view in Fibnet.

Figure 4.9 shows the comparison of the cross section of the numerical model and one obtained by SEM.

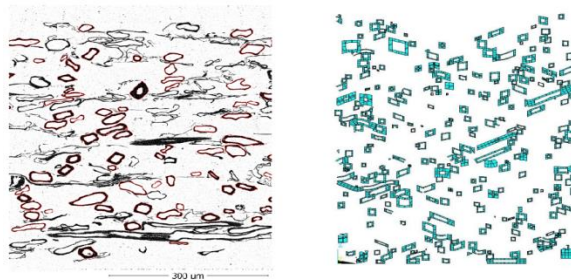


Figure 4.9: Fiber cross section of the network in FibNet.

The average number per cross-section in the model (120) appeared to be closed to the one obtained in the SEM (112), which affirms the adequate representation of fiber geometries. There is apparently larger number of smaller fibers visible in the numerical model, which are difficult to detect in the SEM image.

4.2.1 Fiber model

Each fiber was represented with a number of quadratic Timoshenko beam elements. Despite being a line element, beam element should be integrated over the entire volume in order to capture the gradient in plastic deformation. Each beam is partitioned into quadrilateral segments which form the hollow rectangular cross-section. Each segment has four integration points at which the material response is evaluated and is used to calculate the tangent stiffness needed in implicit finite element method. The area integration is followed by the integration along the element. Figure 4.10 shows how the fibers are partitioned into segments.

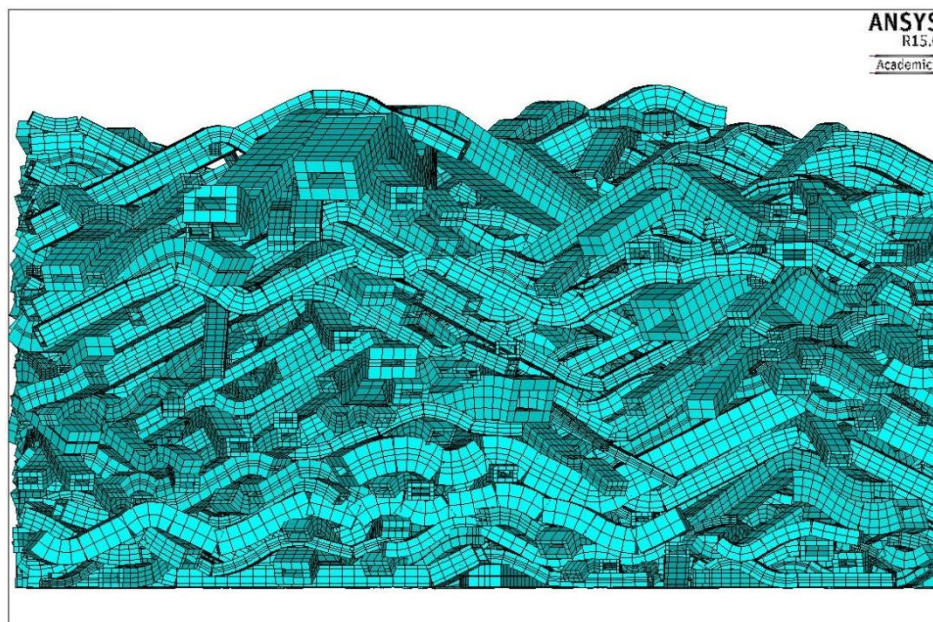


Figure 4.10: 5mm x 1 mm network close view in Fibnet.

4.2.2 Contact model

In the dry fiber network simulation, we assumed the fibers bonded together the bonds may delaminate under a prescribed load. The contact between the fibers was described with beam-to-beam contact. For the reference network model, the contact properties in Table 4.1 was used. The stiffness values obtained from the bond model as described per Chapter 3. The bond strength was estimate by tensile test results. The separation distances were calculated by using bilinear cohesive zone modeling of contact debonding with 1.15 of separation coefficient, the stiffness and the bond strength.

Table 4.1: Fiber contact properties.

Normal Bond Strenght [mN]	Tangential Bond Strenght [mN]	Normal Seperation Distance [μm]	Tangential Seperation Distance [μm]	Normal Bond Stiffness [kN/m]	Tangential Bond Stiffness [kN/m]
160	32	13.6	7.1	14.5	5.57

4.2.3 Material

We use bilinear isotropic hardening plasticity for beams to describe constitutive relations at the fiber level. This model requires elastic and shear modulus of the fiber, yield stress and the tangent modulus. These parameters were estimate using a detailed fiber model, described elsewhere, [16] assuming that the average micro-fibril orientation of the fibers is 23 degrees and the fraction of lignin is 55%. The following average parameters were assigned to the fibers.

Table 4.2: Fiber mechanical properties.

Young's modulus [GPa]	Tangent modulus [GPa]	Yield stress [MPa]
18	4.4	220

4.2.4 Boundary conditions

We constrained the network at one end and applied the prescribed displacement at another end as demonstrated in Figure 4.11.

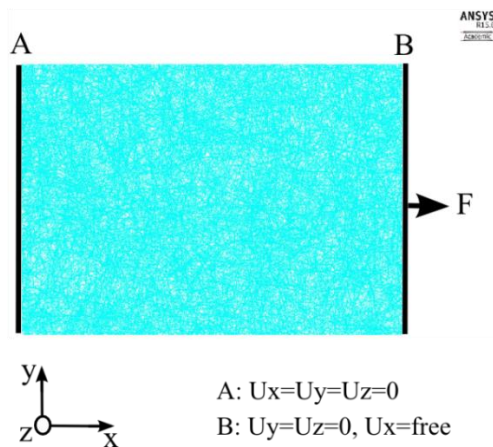


Figure 4.11: Adopted boundary conditions.

4.2.5 Results

Network size dependency

As we work with a relatively small size of the network, it is natural to investigate the size effect first. Figure 4.12 shows network the size dependency with respect to length and width changes. It can be seen that the length of the network has relatively small effect on the stress-strain curve. The width effect has a greater impact presumably due to changes in mean values of fiber length, but once the width reaches 5-6 mm, the relative changes become negligible. We chose the network size, of 7.5mm x 5 mm for all the parametric studies.

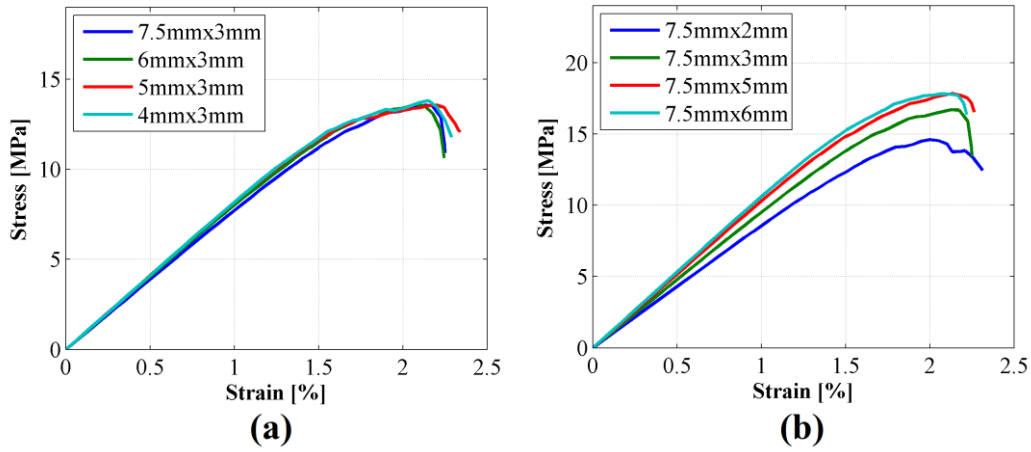


Figure 4.12: Fiber network size dependency: a) length b) width.

Size dependency on this scale takes place in the paper tensile test if there is strain localization on the paper. However, as we demonstrated in our in DSP tests (Section 2.5), we could not observe significant strain localization in sheet, presumably due to relatively short fiber having low number of contacts in the considered sparse sheets.

Effect of Bond Strength

The effect of bond strength is fairly large on the network strength as shown in Figure 4.17. Increasing bond strength by factor two increases the tensile strength nearly by the same factor. The stiffness of the network was unaffected and the curve begins to deviate close to the failure point.

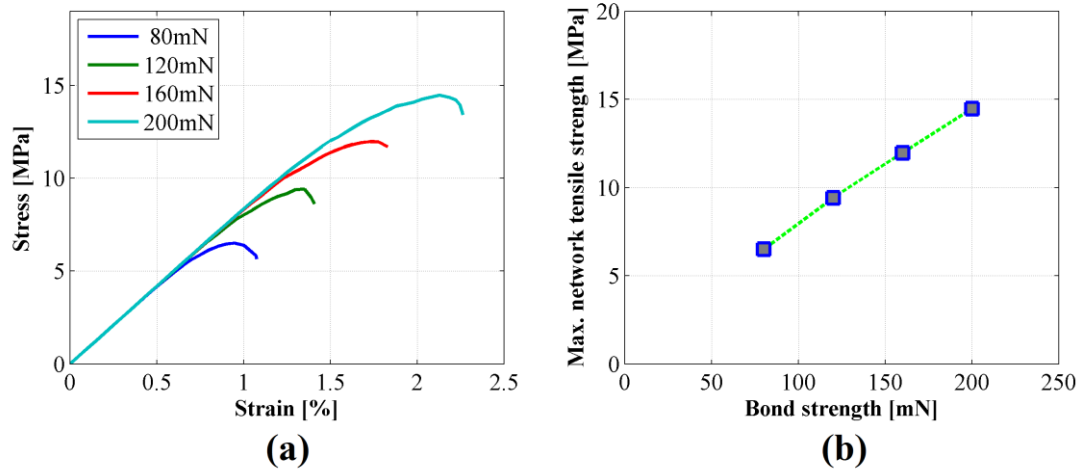


Figure 4.13: The effect of the bond strength.

Bond stiffness

Figure 4.14a shows the effect of bond stiffness. Decreasing the bond stiffness affects the strain to failure and the elastic modulus. It is a first indicator that there is a large fraction of elastic energy stored in the bonds themselves which is also shown in Figure 4.14b, that shows how the elastic energy stored in the network is partitioned between different forms of deformation. Almost half of the elastic energy is stored in the bonds. This was not the case with denser sheets considered by Borodulina [13]. This confirms that the number of bonds in the considered sheets is far lower than that in the denser sheets with Kraft fibers considered in the previous studies. As the number of bonds decreases, the relative changes in their number make greater differences.

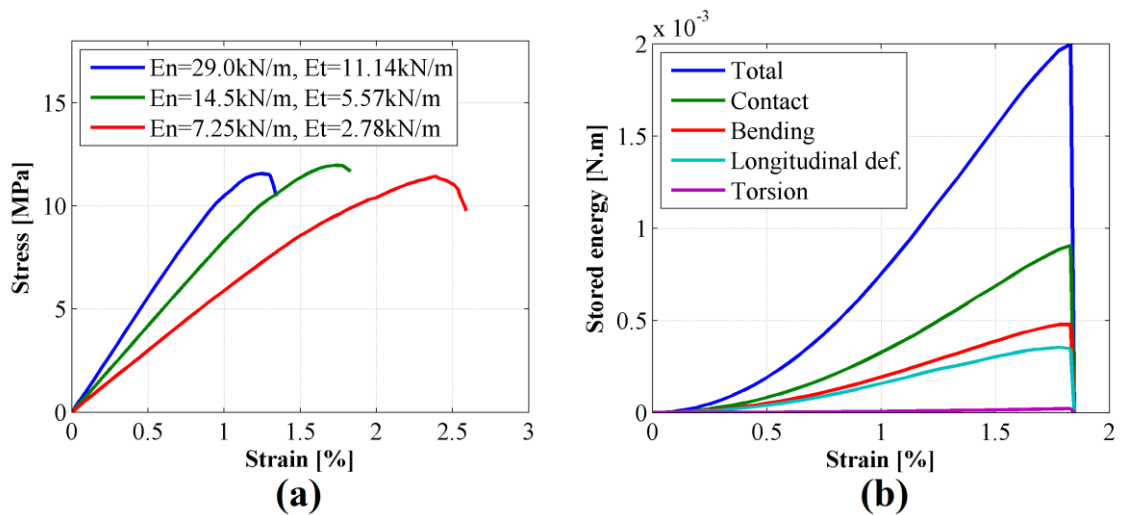


Figure 4.14: a) The effect of the bond stiffness b) Stored elastic energy in the network.

Effect of bonded area through the area of contact

The relative bonded area can affect the bond strength and bond compliance. As mentioned earlier, the effect of the bond area on the bond strength was outside the scope of this work as it would require the extension of the detailed bond model with debonding mechanisms. We only examined the effect of the bond area through its influence on the bond compliance. We used the FE bond model and reduced the bonded regions from 100% to 35% and 15% (see Figure 3.24-3.25). The calculated normal and shear bond stiffness were then used in the network simulation. Figure 4.15 shows that, bonded area of the fibers has minor effect on network strength through its effect on the bond compliance.

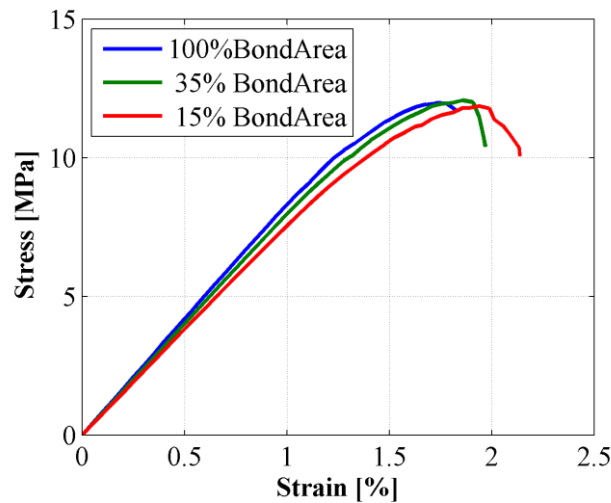


Figure 4.15: The effect of the bonded area through its influence on bond compliance.

Effect of bonded area through the number of contacts

Another way of changing the relative bonded area is changing the number of contacts. We removed the existing bonds in the network to study the effect of the number of bonds. Figure 4.16 shows that the number of bonds has a significant effect on both the stiffness and the strength. The strain to failure did not change significantly. Again, this is different to the results from a denser sheet. It shows again that having initial low number of bonds will make any change related to the bond stiffness to be reflected in the network stiffness.

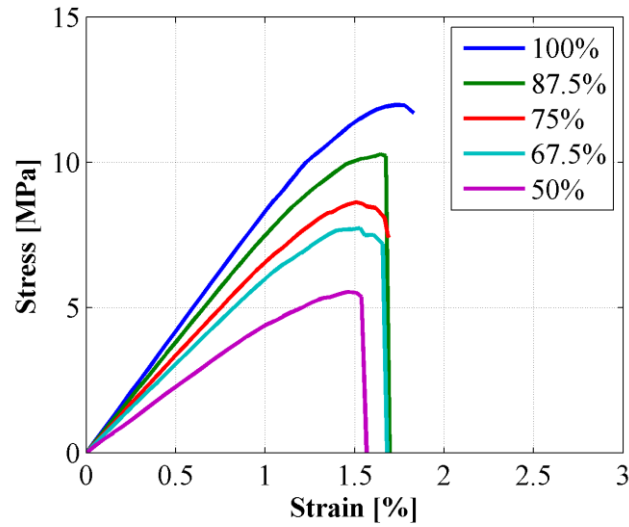


Figure 4.16: The effect of the number of bonds onto the stress-strain curves.

Comparison simulation with experimental results

In this section we will investigate the applicability of the AFM measurements, which showed that the adhesion force is almost unaffected by the modification, while the stiffness was changed significantly. The treated fibers had lower stiffness. We will therefore independently change the bond strength (both in normal and tangent direction) and bond stiffness with respect to the reference case. The change will be done by the ratio between separation energies from the treated and untreated fibers. Figure 4.17 shows five curves: two from the experiments on the treated and untreated samples, and three from the simulations. In the simulation results we showed the reference case and two modifications: one with increased stiffness and another one with decreased bond strength. Both of these scenarios are plausible and will represent the removal of the strength additives. The results show, however, that the bond stiffness is change affects the stiffness of the entire network, which does not happen in the experiments. The increase of the bond strength does not affect the stiffness and affected the stress-strain curves in a way similar to the experiments. This suggests that the strength additive has increased the bond strength rather than affected the fiber properties. We can also extend the conclusion to the number of bonds, which, as demonstrated earlier, affects the network stiffness too, which is not observed in the experiments.

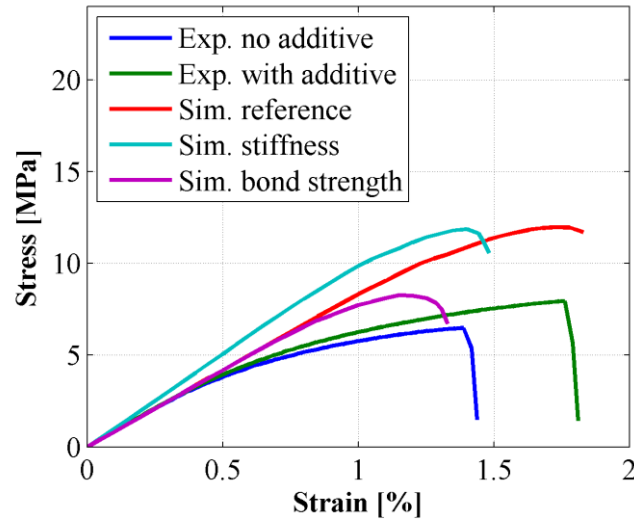


Figure 4.17: Relative comparison of the simulation results with experimental data.

The computation results overshoot the tangent slope of the curve. There are two reasons potential reasons that can be behind this, namely, the size effect and the fiber behavior. As the size increases the strength goes down after surpassing certain size. This effect, however, cannot explain the observed differences in tangent stiffness. Therefore, the dominant reason of this discrepancy resides in the fibers as they control both the primary elastic and the secondary tangent slope of the response. The tangent slope can be affected by the presence of the initial damage within the fiber wall or by the differences between assumed and actual percentage of cellulose in the fibers. Furthermore, as it was shown in the SEM images, the CTMP fibers have considerable S1 layer, which was not included in the fiber model. Finally, the classical relation between the axial and bending stiffness of the fiber may not be obeyed because the fiber does not have a homogeneous structure assumed by the theory. The follow-up study should give attention for a more detailed experimental CTMP fiber characterization and numerical validation of the relation between axial and bending stiffness.

Part 5

Discussion and conclusions

This work was about the effect of the strength additives on a sparse CTMP sheets. We used the modelling to investigate the mechanisms of strength increase and whether the AFM testing can be used as a tool for predicting the effect of the additives.

The fiber and bond parameters needed for the modelling were derived by developing and utilizing the detailed model of the fiber and fiber bond. By using it, we obtained fiber elastic modulus, fiber yield stress, fiber tangent modulus and the contact stiffness in the tangent and normal directions. The bond strength was estimated in a way to obtain relatively the same strain to failure as was recorded in the experiments. An alternative estimation of the bond strength directly from the numerical model has not been undertaken in this work. The network structural characteristics needed for reconstructions were obtained by SEM images. All the mechanical tests and characterizations were performed by KTH in collaboration with Innventia AB. The fiber length and curl characterization was performed with FiberLab at PTS as a part of the PowerBonds project.

By using the detailed fiber model, we found that the parameter that affects the bond stiffness the most is the wall thickness. The greater the wall thickness is the larger the stiffness of the bond region. We also found that pressing the fiber increases the stiffness. At the same time, the diameter surprisingly has a rather limited effect with a given wall thickness. Tangent and normal stiffness of the bond follow the same trends apart from the influence of MFA and orientation of the bond. While MFA has a large influence on the tangent stiffness and limited influence on the normal stiffness, the bond orientation shows a different trend, affecting both the normal and tangent stiffness. The area of individual bond contact did not affect the bond stiffness significantly.

By using the network model, we found that with a given paper structure, both the bond stiffness and the number of contacts have a tremendous influence on network stiffness. It can be explained by a relatively low density of the network, which brings the number of contacts to the point, where the relative changes becomes influential. Also it shows that there is a large fraction of elastic energy stored in the bonds, this means that changing the pulp wall thickness and dimensions or number of contacts will affect the sheet stiffness at a given density. Due to the network stiffness being sensitive to the

changes, we observed interesting trends: changing the number of bonds did not affect the strain to failure but only strength, while changes in bond stiffness affected the strain to failure and not the strength. Increasing the bond strength, on the other hand, expectedly improved the strength of the sheet without affecting the stiffness.

The direct comparison of the modelling and experimental results led to the conclusion that the strength additives improves the bond strength only leaving the number of bonds and the bond stiffness practically intact. This conclusion undermines the applicability of the AFM results, which were unable to predict the changes in the adhesion force. There are also some uncertainties regarding the measurements, such as the influence of the drying history of estimating the area of contacts, as the exact surface characteristics required for that and the mechanics of the testing remain unclear. We therefore recommend being cautious in interpreting the results from the AFM.

5.1 Future work

Direct estimation of the bond strength from the detailed fiber bond model seem to be the natural step forward for this work allowing to establish a direct connection between relative bonded area and network strength. Currently, it is done implicitly. Looking at the effects of special variability in the bond parameters is another alternative.

References

- 1) R. S. Seth, D. H. Page, and J. Brander, "The Stress Strain Curve of Paper," in *The Role of Fundamental Research in Paper Making*, vol. 1, London: Mechanical Engineering Publication, 1983, pp. 421–452.
- 2) Gurnagul, N., Seth, R.S., "Wet-web strength of hard wood kraft pulps," *Pulp & Paper Canada* 98, 1997, 44-48.
- 3) Retulainen, E., Nieminen, K., "Fibre properties as control variables in papermaking? Part 2. Strengthening interfibre bonds and reducing grammage," *Paperi ja Puu*, 1996, 78(5):305-312.
- 4) Kallmes, O. and Corte, H., "The Structure of Paper. I. The Statistical Geometry of an Ideal Two-dimensional Fibre Network," *Tappi*, 43(9), 1960, 737-752.
- 5) Corte, H. and Kallmes, O.J., "Statistical Geometry of a Fibrous Network, In: *Formation and Structure of Paper*," *Trans. 2nd Fund. Res. Symp. Oxford* 1961, 13-46.
- 6) Deng, M. and Dodson, C.T.J., "Paper: an Engineered Stochastic Structure," *TAPPI Press*, 1994.
- 7) Bronkhorst, C.A., "Modeling Paper as a Two dimensional Elastic-plastic Stochastic Network," *Int. J. Solids Struct.*, 40(20), 2003, 5441-5454.
- 8) Heyden S., "Network Modeling for the Evaluation of Mechanical Properties of Cellulose Fibre Fluff," PhD thesis, Lund University, Lund, Sweden, 2000.
- 9) Heyden, S. and Gustafsson, P.J., "Stress-strain Performance of Paper and Fluff by Network modelling," In: *The Science of Papermaking*, *Trans. 12th Fund. Res. Symp. Oxford* 2001, Bury, UK, PPFRS, 1385-1401
- 10) Nilsen, N., Zabihian, M. and Niskanen, K., "KCLPAKKA: a Tool for Simulating Paper Properties," *Tappi J.*, 81 (5), 1998, 163-166.
- 11) Kulachenko, A. and Uesaka, T., "Simulation of Wet Fiber Network Deformation," *Progress in Paper Physics*, Montreal, Canada, 2010.
- 12) Zavarise, G. and Wriggers, P., "Contact with friction between beams in 3-D space," *International Journal for Numerical Methods in Engineering* 49, 2000, 977-1006.
- 13) Borodulina, S., Kulachenko, A., Galland, S., Nygård, M., "Stress-strain curve of paper revisited," *Nord. Pulp Pap. Res. J.*, 27(2), 2012, 318-328.

- 14) Vesterlind, E. & Höglund, H., “Chemitermomechanical pulp made from birch at high temperature,” Nordic Pulp & Paper Research Journal, vol. 21: 2, 2006, ss. 216-221.
- 15) Kaarlo Niskanen (Editor), Paper Physics (Papermaking Science and Technology).
- 16) Tom Lindström, Lars Wågberg and Tomas Larson, “On the nature of joint strength in paper,” Innventia, 2005.
- 17) S. Borodulina, A. Kulachenko, “Constitutive modeling of a paper fiber in cyclic loading applications,” Department of Solid Mechanics, The Royal Institute of Technology (KTH), SE-100 44 Stockholm, Sweden, 2013.
- 18) K.Persson, “Micromechanical modelling of wood and fiber properties,” PhD Thesis, Lund University, 2000.

Appendix

1. Digital Speckle Photography (DSP) manual

Introduction

Digital speckle photography (DSP) is performed by correlation of the deformation measurement system Vic 2D (LIMESS®) and Single Column Table Top Instron 5944. The high-resolution camera takes a series of photo frames from the paper surface while applying tensile load to the sample. Later, the software measures the relatively change at the points on the paper sample between frames and assigns local surface strain values to each photo instant.

Operation Steps

1. Make sure that the surface of your sample is in front of the camera. Otherwise, release screws (#2 in Fig.1) and pull the metal sticks (#1 in Fig.1) to turn the holders. Later, put the metal in the available hole and tighten up the screws.

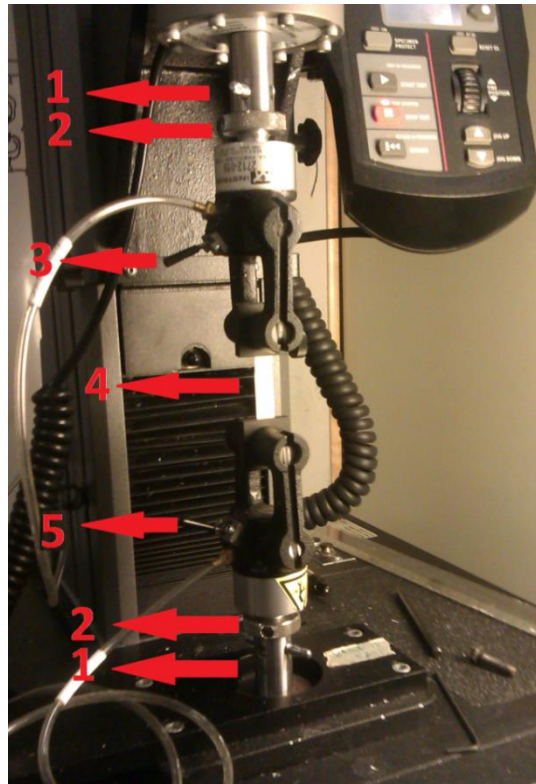


Figure 1

2. Set the camera on the tripod. Push the grey bottom on the arm (#1 in Fig.2) and take it to the right side. Once you place the camera on it, the arm will go to left side automatically.
3. Set the camera as parallel to the ground. Check if the bubble (#2 in Fig.2) is in the middle of the circle. If it is not, use the tripod arms to set it in the middle of circle.

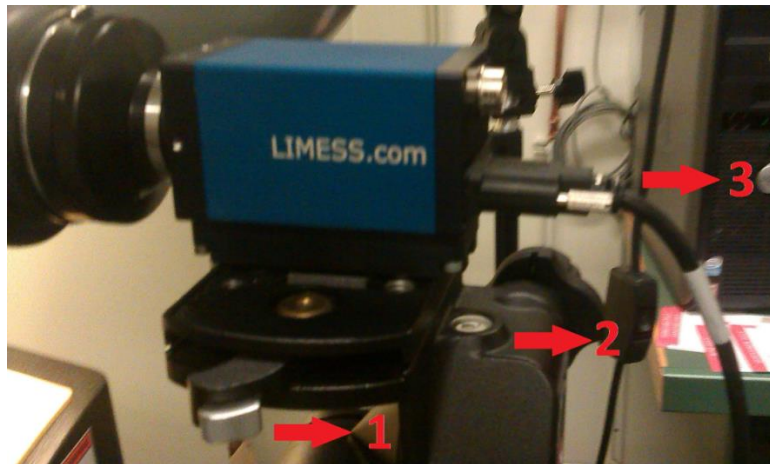


Figure 2

4. Turn on the tensile machine by a button in the back of the machine.
5. Open *Bluehill 2* software on the computer next to the tensile machine. Pass error message by continue.
6. Once the software is open, make “set zero adjustments of the holders”. Use #1 in Fig. 3 to let the holders around 2 mm close. After this point, use fine position (#2 in Fig. 3) to let the holders closer until you see any small increment in the force and **BE CAREFUL** when you adjust the holder so that **THEY DO NOT TOUCH EACH OTHER**. Push set zero button (#3 in Fig.3).
7. Set the holders to your specimen length. Use #1 in Fig.3 to set the holders' distance to 30 mm (our specimen) and push set zero again (#3 in Fig.3).

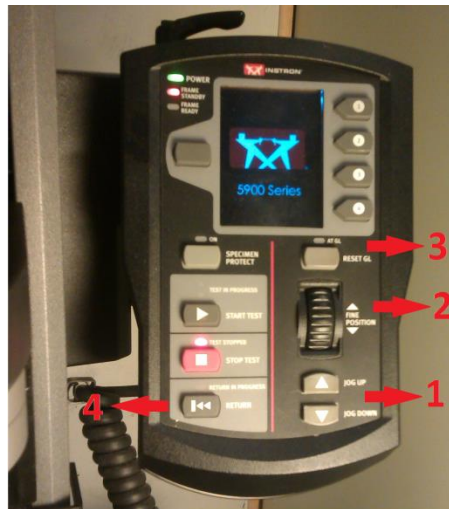


Figure 3

8. Place your sample in tensile test machine. Switches are shown as #3 and #5 in Figure 1. Place your sample by using the only upper clamp with upper switch (#3 in Fig.1). Keep the bottom clamp open (#5 in Fig.1).
9. Go to the software on the computer of the tensile test machine to open new tensile test. Select > Test > Browse > find the designated directory and double click it.
10. Open a new file in C: > Document and settings > All user > Method > and give a name.
11. Go to Browse.
12. Fill the sample labels, Length 30mm, thickness, width and time capture (500 for us) in the acquisition blank.
13. Click Balance up.
14. Close the bottom clamp with the switch below (#5 in Fig.1).
15. Once you close the below the clamp, the specimen will buckle, and you will see minus force. Use fine control (#2 in Fig.3) to come as close as possible to zero force.
16. Place the card of the camera (#3 in Fig. 4) into the Laptop. Plug the adapter cable (#2 in Fig.4) and the camera cable on the card of the camera. Plug the adapter to electricity. Plug the other side of camera cable to the camera (#3 in Fig.2) and open the laptop.

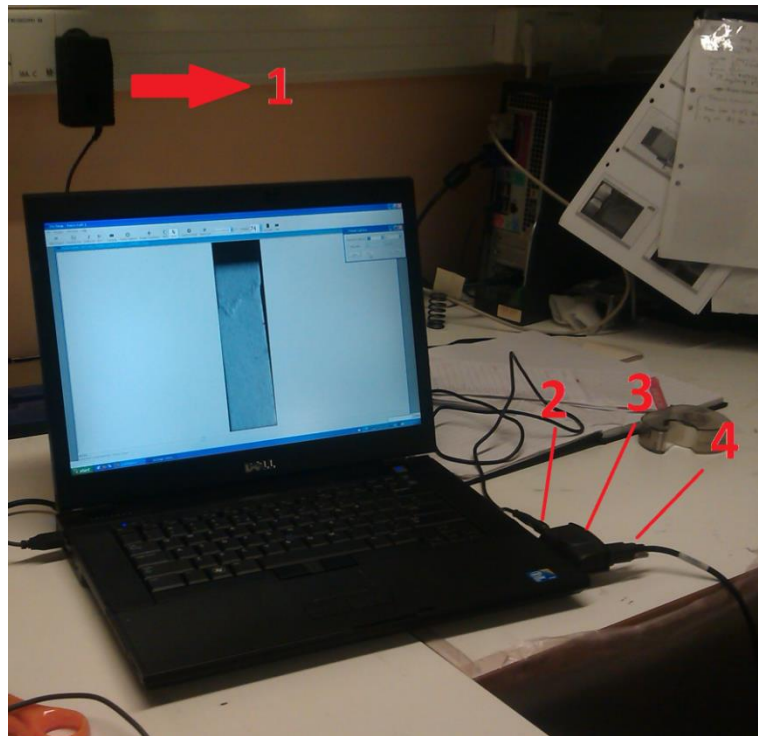


Figure 4

17. Open *Vic-Snap 2009* software in the laptop. Make new folder
18. Select where to save and write a name in the first blank.
19. Open the lens cap.
20. Open light on your sample (#1 in Fig.5).
21. Adjust the zoom (#2 in Fig.5), focus (#3 in Fig.5) and light (#4 in Fig.5) while you check your sample on the laptop screen. To have more precision, make the zoom on the laptop screen and adjust it again. Also you can clip the view of the specimen on the screen.



Figure 5

22. Enter time capture (500 for us) in acquisition. Be careful, this must be the same in both the laptop and the computer. **Don't press OK before following step!**
23. When you say *OK*, the software starts to capture the frames. But mostly first 5-10 frame is not useful so once you say *OK* wait until first 5-10 frames (you see the image number on the software interface) and then start the tensile test on the computer with the *START* button.
If the software in the laptop does not start to count image;
 -Try to click *START* and *STOP* a few times
 -If it still does not work, try to restart the software.
Never start the tensile test unless the software in the laptop comes 5-10 image numbers.
24. If you have a new sample to measure,
 Edit project > make a new folder > ok. Make sure the image counting box is empty.
25. Take your sample from the clamps.
26. Click *RETURN* button (#4 in Fig.3) to go to the old position.
27. Click *NEXT* in the tensile machine computer.
28. Go to steps 8, then 13, 22 and 23
29. If you finish your measurements, click *FINISH* Check export raw data and export results> next > finish sample
30. Close the software in the tensile machine computer.
31. Close the tensile test machine from back.
32. Fill the log book.
33. Open *Vic-2D* software in the laptop. Select Speckle Image. Go 3 steps back, find the folder Artem. Select All and open.
34. Click rectangle (#1 in Fig.6a) and select all specimen surface (see Fig.6b) that you need. Carry the 3rd green point (Seed points) to below of middle as it is shown in Fig.6b. The algorithm uses these points or relatively displacement. Correlation algorithm uses the results from the seed point to obtain an initial guess for second point analyzed and continue in this manner until all points in algorithm of image are analyzed.
35. Change the subset (#2 in Fig.6a) to 31. Change step size to 1 for high resolution which means each pixel will be considered in analyses. For instance, if you select 2, then each second pixel will be considered.
36. Start the analyses by click run (#3 in Fig.6a).
37. When it is done, click close on the front window.
38. Click Data (#4 in Fig.6a) and double-click first data.
39. Click Inspect rectangle (#1 in Fig.6c), select all surfaces of the sample and click extract (#2 in Fig.6c).

40. When the new window appears, click save data. Once you see export data window, select the necessary data to extract like strain in x, y and xy directions (exx,eyy,exy) and click Ok. Select file name with “.out” extension and say *OK*. Z direction is not necessary since it is 2D analyses of surface. Also, in this experiment, only strain in y direction is meaningful.
41. Save the project (#5 in Fig.6a).
42. Close the software and the laptop.

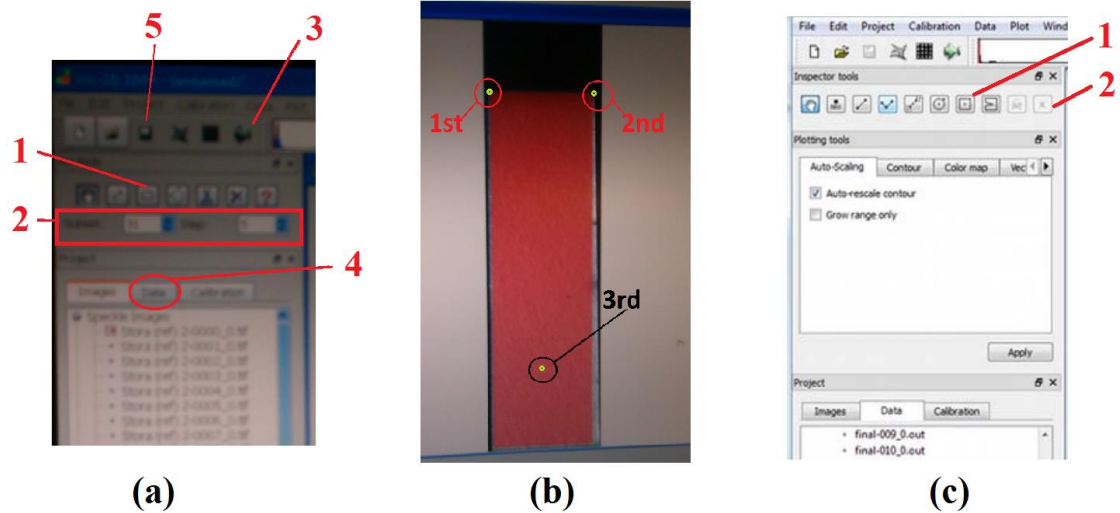


Figure 6

